
Unsupervised Continual Learning for Amortized Bayesian Inference

Aayush Mishra¹

Šimon Kucharský¹

Paul-Christian Bürkner¹

¹Department of Statistics, TU Dortmund University, Germany

Abstract

Amortized Bayesian Inference (ABI) enables efficient posterior estimation using generative neural networks trained on simulated data, but often suffers from performance degradation under model misspecification. While self-consistency (SC) training on unlabeled empirical data can enhance network robustness, current approaches are limited to static, single-task settings and fail to handle sequentially arriving data or distribution shifts. We propose a continual learning framework for ABI that decouples simulation-based pre-training from unsupervised sequential SC fine-tuning on real-world data. To address the challenge of catastrophic forgetting, we introduce two adaptation strategies: (1) SC with episodic replay, utilizing a memory buffer of past observations, and (2) SC with elastic weight consolidation, which regularizes updates to preserve task-critical parameters. Across three diverse case studies, our methods significantly mitigate forgetting and yield posterior estimates that outperform standard simulation-based training, achieving estimates closer to MCMC reference, providing a viable path for trustworthy ABI across a range of different tasks.

across a large number of observations, effectively amortizing the cost of inference over many queries.

Despite its efficiency, ABI remains sensitive to model misspecification and domain shifts, which can severely degrade accuracy of neural posterior estimates. Consequently, a growing body of work focuses on improving the robustness of ABI [Huang et al., 2023, Wehenkel et al., 2024, Schmitt et al., 2023b, Mishra et al., 2025, Elsemüller et al., 2025]. One promising direction is the use of Bayesian self-consistency losses [Schmitt et al., 2023b, Mishra et al., 2025, Kucharský et al., 2025] which enforce consistency between the learned posterior approximation and the generative model using unlabeled real-world data.

Up until now, existing robustness approaches including self-consistency losses implicitly assume a static or single-task setting. However, in many real-world applications, data arrive sequentially over time rather than being available all at once, such as galaxy observations from different telescopes [Ghosh et al., 2023, Tian et al., 2025], gravitational-wave detections [Abbott et al., 2023], and medical imaging across devices [Wu et al., 2024]. In other contexts, the same ABI model may be used for inference across a range of different scientific domains.

This motivates continual learning (CL) approaches, as re-training models from scratch each time new data become available is computationally expensive, often impractical, and diminishes the pay-off of amortization. CL aims to enable models to acquire new knowledge from incoming data while preserving performance on previous data, thereby mitigating the problem of catastrophic forgetting [Wang et al., 2024, Van de Ven and Tolias, 2019, Parisi et al., 2019, Rolnick et al., 2019]. Referring to the sequential incoming datasets as *tasks*, the central challenge lies in ensuring that learning new tasks does not overwrite the representations or network parameters critical for earlier tasks. CL also enables the network to transfer knowledge from earlier tasks, improving data efficiency when adapting to new tasks through shared representations and replay mechanisms

1 INTRODUCTION

Amortized Bayesian Inference [ABI; Radev et al., 2023, Schmitt et al., 2023a, Elsemüller et al., 2023, Zammit-Mangion et al., 2025, Gloeckler et al., 2024, Deistler et al., 2025, Wildberger et al., 2023] addresses computational limitations of traditional Bayesian inference methods by training generative neural networks to approximate posterior distributions over parameters θ using simulated pairs of data x and parameters θ from a probabilistic model $p(\theta, x)$. Once trained, these networks enable fast, near-instant inference

[Rolnick et al., 2019, Parisi et al., 2019].

This article makes the following contributions:

- We propose a two-stage training for ABI that decouples supervised simulation-based training from unsupervised self-consistency training on empirical data, allowing us to fine-tune networks for new incoming tasks in an unsupervised CL setting.
- We demonstrate a key failure mode of ABI: when applied sequentially across tasks, naive self-consistency updates can cause catastrophic forgetting.
- We introduce **self-consistency with episodic replay**, a CL method that mitigates catastrophic forgetting by retaining a small buffer of data from previous tasks; we further provide a memory-budgeted variant that uses clustering to preserve diversity of training data while keeping memory requirements constant.
- We introduce **self-consistency with elastic weight consolidation**, an unsupervised regularization based approach which prevents catastrophic forgetting by constraining weights important for previous tasks while allowing less critical parameters to adapt flexibly to new tasks.
- We further examine a unified objective that combines episodic replay and elastic weight consolidation with self-consistency, enabling us to analyze the combined effects of both CL mechanisms.
- Across three case studies, we demonstrate that the proposed methods substantially improve accuracy of posterior approximations on empirical data across different tasks against simulation-based training. Further, we show that our unsupervised continual learning approaches effectively mitigate catastrophic forgetting.

2 METHODS

2.1 NEURAL POSTERIOR ESTIMATION

We consider the general Bayesian inference problem of estimating parameters θ from data x addressed by means of generative neural networks. The posterior is defined by Bayes’ rule, $p(\theta | x) \propto p(\theta, x) = p(x | \theta)p(\theta)$, where $p(\theta)$ is the prior and $p(x | \theta)$ the likelihood. ABI casts posterior inference as a supervised learning problem. It learns a conditional distribution $q_{\Phi}(\theta | x)$, via a neural network with weights Φ , to approximate the posterior $p(\theta | x)$ by optimizing a simulation-based (SB) loss of the form

$$\mathcal{L}_{\text{SB}}(\Phi) = \mathbb{E}_{(\theta, x) \sim p(\theta, x)} [J(q_{\Phi}(\cdot | x), \theta)]. \quad (1)$$

Here, J is a strictly-proper scoring rule such as maximum likelihood loss for discrete normalizing flows [Papamakarios et al., 2021, Kobyzev et al., 2020] or vector-field loss

for flow-matching [Lipman et al., 2022]. As we require fast density estimation for losses used for CL training, we use discrete normalizing flows via invertible neural networks. The neural networks to be optimized are a generative network q and (optionally) a summary network h extracting lower dimensional sufficient statistics from the data. These networks are optimized using the maximum-likelihood loss

$$\mathcal{L}_{\text{SB}}(\Phi) = \mathbb{E}_{p(\theta, x)} [-\log q_{\phi}(\theta | h_{\psi}(x))], \quad (2)$$

where $\Phi = (\phi, \psi)$ denotes the collection of all trainable parameters of the network. We approximate the expectations in Eq. 2 with finite simulated data as

$$\mathcal{L}_{\text{SB}}(\Phi) \approx -\frac{1}{N} \sum_{n=1}^N \log q_{\phi}(\theta_n | h_{\psi}(x_n)). \quad (3)$$

where $(\theta_n, x_n) \sim p(\theta, x)$ are simulations from the joint probabilistic model.

While simulation-based training performs well when a large amount of simulated training data is available and the underlying model is correctly specified, its estimates can be highly inaccurate when either of these conditions is not met [Huang et al., 2023, Schmitt et al., 2023b, Wehenkel et al., 2024, Mishra et al., 2025]. Consequently, training solely on samples from the prior predictive distribution may be insufficient to ensure robust posterior estimates. Since Bayesian self-consistency losses described below can be applied to empirical data rather than simulated data from the prior predictive distribution, they are suitable to overcome these limitations of standard simulation-based training.

2.2 BAYESIAN SELF-CONSISTENCY LOSSES

Bayesian self-consistency (SC) losses [Schmitt et al., 2023b, Mishra et al., 2025, Kucharský et al., 2025, Köthe, 2023, Richter et al., 2020, Richter and Berner, 2023, Sanokowski et al., 2025] are strictly-proper scores that leverage a simple symmetry in Bayes’ rule to enforce accurate posterior estimation: Under exact inference, the marginal likelihood is independent of the parameters θ . In other words, the Bayesian self-consistency ratio between the likelihood-prior product and the posterior remains constant across any set of parameter values $\theta^{(1)}, \dots, \theta^{(L)}$,

$$p(x) = \frac{p(x | \theta^{(1)})p(\theta^{(1)})}{p(\theta^{(1)} | x)} = \dots = \frac{p(x | \theta^{(L)})p(\theta^{(L)})}{p(\theta^{(L)} | x)}. \quad (4)$$

However, when the true posterior $p(\theta | x)$ is replaced with a neural approximation $q_{\Phi}(\theta | x)$, bespoke ratios will longer be constant for any imperfect approximation. We can equivalently say that the log ratios have positive variance, which readily implies a loss function to be minimized. We will use the unsupervised formulation of the (variance-based) self-consistency loss, which utilizes unlabeled real-world data

[Mishra et al., 2025]. Hereafter, we refer to the variance-based self-consistency loss simply as the “self-consistency loss” or short “SC loss”. For M instances of real-world data $x_m^* \sim p^*(x)$, the SC loss is given by

$$\begin{aligned} \mathcal{L}_{\text{SC}}(\Phi) &= \mathcal{L}_{\text{SC}}(\Phi; x^*) \\ &= \frac{1}{M} \sum_{m=1}^M \text{Var}_{\theta \sim p_C(\theta)} \left[\log p(x_m^* | \theta) + \log p(\theta) \right. \\ &\quad \left. - \log q_\phi(\theta | h_\psi(x_m^*)) \right]. \end{aligned} \tag{5}$$

Here, $p_C(\theta)$ is a parameter proposal distribution, which we set to the current approximate posterior $q_{\phi,r}(\theta | h_{\psi,r}(x_m^*))$ at training iteration r [Mishra et al., 2025].

The SC loss possesses several properties that make it particularly appealing for use in CL scenarios. First, it does not require labeled data, allowing the use of real-world unlabeled data to minimize the SC loss. Second, the SC loss provides additional signal which leads to more accurate posterior estimation even for atypical data [Mishra et al., 2025, Kucharský et al., 2025], where pure simulation-based training fails [Frazier et al., 2024, Ward et al., 2022, Mishra et al., 2025, Schmitt et al., 2023a]. Third, the SC loss can attain accurate posterior approximations with comparatively little training data, making it data-efficient.

2.3 REGIMES OF SELF-CONSISTENCY TRAINING

Prior work has used SC losses in combination with SB losses in a semi-supervised setup during training [Mishra et al., 2025, Kucharský et al., 2025, Schmitt et al., 2023b]. In a CL setting, tasks arrive sequentially $\{\mathcal{T}_1, \dots, \mathcal{T}_T\}$ and observed data from different tasks may not be available at the same time. Further, because the approximate posterior is initially highly inaccurate, the SC loss tends to be numerically unstable at first; this often requires careful weight scheduling of the two losses for stable training [Mishra et al., 2025, Schmitt et al., 2023b, Kucharský et al., 2025].

To address these issues, we split training into two stages. First, we perform standard simulation-based pre-training of the posterior network using the SB loss. After this initial step, the SB loss is no longer used. Second, we train the posterior network using the SC loss as we accrue data from different tasks. Next, we describe different training regimes for using the SC loss on new data, regimes that constitute the main focus of this article.

2.3.1 Test-time Training with Self-Consistency

In the test-time training regime, as data from new tasks arrive, the simulation-based pre-trained network is further trained with the SC loss on data from the current task only.

This is the closest method to the combined SB and SC loss studied in recent work [Mishra et al., 2025, Kucharský et al., 2025]. No CL mechanism is employed; updates are performed solely to improve posterior estimates for the current task, without explicitly retaining performance on other tasks. This setting is particularly advantageous in scenarios where accuracy on the current task is paramount and long-term retention across tasks is not required.

2.3.2 Continual Learning with Self-Consistency

In a CL regime, we use the SC training in a sequential fashion, where at step t , we minimize the SC loss using data from task \mathcal{T}_t for a network that was pre-trained by the SC loss for all previous tasks $\{\mathcal{T}_1, \dots, \mathcal{T}_{t-1}\}$ sequentially (and initially with the SB loss). Crucially, because the SC objective does not explicitly constrain the network on earlier task distributions, updates driven solely by the current task can overwrite representations important for previous tasks. As we later show, this may lead to catastrophic forgetting, and we further call this approach “naive SC”.

2.3.3 Self-Consistency with Episodic Replay

To alleviate catastrophic forgetting in CL, we employ an episodic replay (ER) mechanism [Rolnick et al., 2019, Chaudhry et al., 2019, Shin et al., 2017] that stores unlabeled real-world data from previous tasks $\{\mathcal{T}_1, \mathcal{T}_2, \dots, \mathcal{T}_{t-1}\}$ in a memory buffer \mathcal{E} . During training with self-consistency loss on a new task \mathcal{T}_t , the network is jointly optimized on the current task data and stored samples from \mathcal{E} , encouraging a stability–plasticity balance. This allows the network to retain knowledge of past tasks while adapting to new tasks. The resulting episodic replay based self-consistency (SC-ER) loss is given by

$$\mathcal{L}_{\text{SC-ER}}(\Phi) = \mathcal{L}_{\text{SC}}(\Phi; x_{SC}^*), \tag{6}$$

where $x_{SC}^* = x_t^* \cup \mathcal{E}$, x_t^* represents the data from the task \mathcal{T}_t , and \mathcal{E} contains a subset of data from previous tasks. An additional benefit of using ER is that it preserves the inference target of self-consistency (analytic posterior) [Els Müller et al., 2025], because including replay buffer within the same loss function does not involve any regularization term unlike other CL approaches [Kirkpatrick et al., 2017, Zenke et al., 2017, Aljundi et al., 2018, Li and Hoiem, 2017].

As the number of tasks increase, storing even a few representative samples from each task may become impractical [Rolnick et al., 2019, Li et al., 2024]. To address this, we maintain a minimal replay buffer that initially stores few observations per task. Once the memory capacity is reached, we apply K-medoids clustering [Kaufman and Rousseeuw, 2009] over all stored samples and retain only the cluster representatives. The number of clusters is set to match the

maximum buffer size, ensuring that the replay memory remains within the predefined limit while preserving diversity among stored observations. This diversity preserving approach is suitable to be used in combination with SC as it works on minimal data available per task. The overall procedure is summarized in Algorithm 1.

Algorithm 1 Self-Consistency with Episodic Replay

```

1: Input: Simulated dataset  $(\theta, x) \sim p(\theta, x)$ , unlabeled
   real-world tasks  $\{\mathcal{T}_t\}_{t=1}^T$ , replay buffer size  $K$ 
2: Output: Trained posterior network  $q_\Phi(\theta | x)$ 
3: Initialize  $q_\Phi(\theta | x)$ , replay buffer  $\mathcal{E} \leftarrow \emptyset$ 
4: Simulation based pre-training
5: for each pretraining iteration do
6:   Sample minibatch  $(\theta, x) \sim p(\theta, x)$ 
7:   Update  $q_\Phi$  by minimizing Eq. 3
8: end for
9: CL on real-world tasks
10: for  $t = 1$  to  $T$  do
11:   Obtain current dataset  $x_t^* \sim p_t^*(x)$  from task  $\mathcal{T}_t$ 
12:   Concatenate replay data with current data:
        $x_{SC}^* \leftarrow x_t^* \cup \mathcal{E}$ 
13:   for each SC-ER iteration do
14:     Compute SC-ER loss  $\mathcal{L}_{SC-ER}$  as in Eq. 6
15:     Update  $q_\Phi$  by minimizing  $\mathcal{L}_{SC-ER}$ 
16:   end for
17:   if using clustering then
18:     Draw posterior samples  $\{\theta_t^{(s)}\}$  from  $q_\Phi(\theta | x_t^*)$ 
19:      $\mathcal{E} \leftarrow \text{KMEDOIDUPDATE}(\mathcal{E}, x_t^*, \{\theta_t^{(s)}\})$ : Alg. 4
20:   else
21:     Store a subset of data from  $\mathcal{T}_t$  in  $\mathcal{E}$ 
22:   end if
23: end for
24: Return  $q_\Phi(\theta | x)$ 

```

2.3.4 Self-Consistency with Elastic Weight Consolidation

In certain CL settings, retaining data from previous tasks is impractical due to privacy constraints [Tong et al., 2025] or long task sequences that make replay inefficient as the memory buffer grows linearly with number of tasks [Shin et al., 2017, Rolnick et al., 2019]. In such cases, we propose to use weight regularization, a widely used strategy to mitigate catastrophic forgetting in continual learning [Kirkpatrick et al., 2017, Zenke et al., 2017, Aljundi et al., 2018]. The core idea is to constrain updates to network parameters that are important for previously learned tasks while allowing flexibility for adapting to new tasks. This is achieved by introducing a regularization term in the loss function that penalizes large deviations of the current network parameters from their previously learned values. Formally, after training on task \mathcal{T}_i , the optimized network parameters are denoted by Φ_i^* . When learning a new task \mathcal{T}_t , we minimize

the following objective:

$$\mathcal{L}_{SC-WR}(\Phi_t) = \mathcal{L}_{SC}(\Phi_t) + \lambda \sum_{i=1}^{t-1} \Omega(\Phi_t, \Phi_i^*), \quad (7)$$

where \mathcal{L}_{SC} denotes the task-specific SC loss for \mathcal{T}_t , $\Omega(\cdot)$ is a regularization term that measures the deviation of the current parameters Φ_t from the previous parameters Φ_i^* , and λ is a hyperparameter controlling the trade-off between retaining previous knowledge and adapting to new tasks. We instantiate $\Omega(\cdot)$ as quadratic penalty taking inspiration from Elastic Weight Consolidation [EWC, Kirkpatrick et al., 2017]:

$$\Omega(\Phi_t, \Phi_i^*) = \sum_j \mathcal{W}_{jj} (\Phi_{t,j} - \Phi_{i,j}^*)^2, \quad (8)$$

where \mathcal{W}_{jj} represents the diagonal importance matrix that estimates the importance of parameter $\Phi_{i,j}^*$ for previous task \mathcal{T}_i , and j indexes all trainable network parameters. After convergence on task \mathcal{T}_i , we compute the diagonal information matrix as,

$$\mathcal{W}_{jj}^{(i)} = \mathbb{E}_{x^* \sim p_i^*(x)} \left[\left(\frac{\partial \mathcal{L}_{SC}(x^*)}{\partial \Phi_j} \right)^2 \right], \quad (9)$$

$$\mathcal{W}_{jj}^{(i)} \approx \frac{1}{K} \sum_{k=1}^K \left[\left(\frac{\partial \mathcal{L}_{SC}(x_k^*)}{\partial \Phi_j} \right)^2 \right]. \quad (10)$$

where the expectation in Eq. 9 is approximated from K unlabeled samples from \mathcal{T}_i in Eq. 10. This approach effectively anchors critical parameters while allowing less important ones to adapt freely. As we utilize the SC loss, it allows us to compute parameter importance using only unlabeled real-world data. When training the network on task \mathcal{T}_t , we minimize the following SC-EWC loss:

$$\mathcal{L}_{SC-EWC}(\Phi_t) = \mathcal{L}_{SC}(\Phi_t; x_t^*) + \frac{\lambda}{2} \sum_{i=1}^{t-1} \sum_j \mathcal{W}_{jj}^{(i)} (\Phi_{t,j} - \Phi_{i,j}^*)^2 \quad (11)$$

The overall procedure is summarized in Algorithm 2. We also combine ER and EWC with self-consistency simultaneously to see their combined effects (see Algorithm 3). In such a case, the loss becomes:

$$\begin{aligned} \mathcal{L}_{SC-ER-EWC}(\Phi_t) = & \mathcal{L}_{SC-ER}(\Phi_t; x_{SC}^*) \\ & + \frac{\lambda}{2} \sum_{i=1}^{t-1} \sum_j \mathcal{W}_{jj}^{(i)} (\Phi_{t,j} - \Phi_{i,j}^*)^2 \end{aligned} \quad (12)$$

3 RELATED WORK

CL has been extensively studied in the last decades as overcoming catastrophic forgetting remains a major challenge

Algorithm 2 SC with Elastic Weight Consolidation

```
1: Input: Simulated dataset  $(\theta, x) \sim p(\theta, x)$ , unlabeled tasks  $\{\mathcal{T}_t\}_{t=1}^T$ , EWC weight  $\lambda$ , Fisher batches  $B$ 
2: Output: Trained posterior network  $q_\Phi(\theta | x)$ 
3: Initialize posterior  $q_\Phi$ , EWC record list  $\mathcal{R} \leftarrow \emptyset$ 
4: Simulation-based pre-training
5: for pretraining iterations do
6:   Sample  $(x, \theta) \sim p(\theta, x)$ 
7:   Update  $q_\Phi$  by minimizing Eq. 3
8: end for
9: CL
10: for  $t = 1$  to  $T$  do
11:   Obtain current dataset  $x_t^* \sim p_t^*(x)$  from task  $\mathcal{T}_t$ 
12:   for each SC-EWC iteration do
13:     if  $\mathcal{R} \neq \emptyset$  then
14:       Update  $q_\Phi$  by minimizing  $\mathcal{L}_{\text{SC-EWC}}$  from Eq. 11
15:     else
16:       Update  $q_\Phi$  by minimizing  $\mathcal{L}_{\text{SC}}$  from Eq. 5
17:     end if
18:   end for
19:   Estimate  $\mathcal{W}_{jj}^{(t)}$  for task  $\mathcal{T}_t$  as per Eq. 10
20:   Snapshot parameters  $\Phi_t^*$ 
21:   Append  $(\Phi_t^*, \mathcal{W}_{jj}^{(t)})$  to EWC record list  $\mathcal{R}$ 
22: end for
23: Return  $q_\Phi(\theta | x)$ 
```

in deep learning. Three major families of approaches have emerged: (1) Regularization-based methods [Kirkpatrick et al., 2017, Zenke et al., 2017, Aljundi et al., 2019, Kozal et al., 2024, Zhao et al., 2024, Lewandowski et al., 2025, Gomez-Villa et al., 2024] constrain important network parameters from changing too much. (2) Replay-based methods Lee et al. [2019b], Rolnick et al. [2019], Chaudhry et al. [2019], Aghasanli et al. [2025], Yoo et al. [2024], Madaan et al. [2021] combine current data with stored or generated samples from past during training. (3) Parameter-isolation and architectural approaches [Rusu et al., 2016, Lu et al., 2024, Schwarz et al., 2018, Rao et al., 2019] allocate dedicated sub-networks or dynamically expand networks to prevent forgetting. In this work, we utilize a replay and a regularization based CL approach. We do not include architecture expansion methods, as their parameter growth scales with the number of tasks [Rusu et al., 2016]. Also, such approaches typically restrict parameter sharing across tasks, limiting positive transfer when tasks are related.

Recent work has increasingly investigated robustness in ABI and, more broadly, simulation-based inference [Delaporta et al., 2022, Frazier et al., 2024, Gloeckler et al., 2023]. These approaches can be broadly grouped into two categories: (i) methods that analyze or detect discrepancies between simulated and real-world data [Schmitt et al., 2023a, Alvey et al., 2026, Cannon et al., 2022], and (ii) methods that directly mitigate the impact of simulation gap

on posterior estimation [Ward et al., 2022, Huang et al., 2023, Gloeckler et al., 2023, Wehenkel et al., 2024, Mishra et al., 2025, Elsemüller et al., 2025, Kucharský et al., 2025]. Our work falls into the latter category. Within this line of research, regularization-based approaches [Gloeckler et al., 2023, Huang et al., 2023] introduce additional constraints to correct the posterior estimates. Other approaches such as Wehenkel et al. [2024] incorporate limited real-world labeled data to supplement the simulation-based training, or apply unsupervised domain adaptation techniques to handle distribution shifts [Elsemüller et al., 2025]. More recently, SC-based approaches enhance robustness under model misspecification with unlabeled real-world data [Mishra et al., 2025, Kucharský et al., 2025].

To the best of our knowledge, no prior work has explored CL for ABI, a gap that we address. Existing methods in ABI assume either simultaneous availability of real-world data at training time or that future tasks come from the same distribution, thereby lacking the mechanisms to prevent catastrophic forgetting. By explicitly formulating unsupervised CL within the ABI framework and leveraging SC alongside replay and regularization-based CL strategies, our approach effectively mitigates catastrophic forgetting and improves posterior estimation across sequential tasks.

4 EXPERIMENTS

Experimental setup We conduct three experiments ranging from linear regression to time-series and racing diffusion models. For each experiment, we initially perform simulation-based training of the posterior network using the SB loss in an online setting, which also acts as a baseline. We then train the posterior network sequentially across all tasks in an unsupervised CL setting using our proposed methods (SC-ER, SC-EWC, and SC-ER-EWC) along with naive SC. After completion of training on the final task, we evaluate every method on all the tasks. To assess the capacity of the network for accurate performance on each individual task, we contrast results of the CL methods with test-time SC trained on each task. This directly reveals the extent to which each method mitigates (or fails to mitigate) catastrophic forgetting. All experiments are conducted with the Python library BayesFlow [Kühmichel et al., 2026].

Metrics We use MCMC-based posterior estimates via Stan [Carpenter et al., 2017] as a non-amortized gold-standard throughout our experiments. We measure mean bias as the difference between the posterior mean estimated by different methods and the posterior mean obtained using Stan. Analogously, standard deviation bias quantifies discrepancies in posterior uncertainty. We also compute the Maximum Mean Discrepancy [MMD; Gretton et al., 2012] between posterior samples from our method and those from Stan, using a Gaussian kernel. For better interpretability, we

report the ratio of MMD of a specific method to MMD of the SB training baseline. MMD ratio values smaller than one indicate improved performance compared to the baseline.

4.1 EXPERIMENT 1: LINEAR REGRESSION

First, we consider a standard Bayesian linear regression model with five predictors and $N = 100$ observations. The generative model is

$$y_n \sim \mathcal{N}(\alpha + \mathbf{x}_n^\top \beta, \sigma^2), \quad (13)$$

where α is the intercept, $\beta \in \mathbb{R}^5$ are the regression coefficients, and σ is the observation noise. We place independent priors on all parameters:

$$\begin{aligned} \alpha &\sim \mathcal{N}(0, 1), & \sigma &\sim \text{HalfNormal}(1), \\ \beta &\sim \mathcal{N}(\mathbf{0}, \text{diag}(\tau^2)), & \tau &= (1, 1, 1, 1, 1). \end{aligned} \quad (14)$$

The above model produces a diagonal covariance structure for the slope parameters. Training was performed as described in the experimental setup. For CL, we utilize nine real-world publicly available datasets (see Appendix B) which constitute 9 CL tasks $\{\mathcal{T}_1, \dots, \mathcal{T}_9\}$. We further divided these datasets in ten subsets each having $N = 100$ observations. We also utilize one simulated dataset $\{\mathcal{T}_0\}$, where the ten subsets are independently drawn from prior predictive distribution. For SC-ER replay buffer, we only utilize one subset per task.

Results In Figure 1, we report the MMD ratio across the ten tasks for naive SC, test-time SC, and the proposed SC-ER, SC-EWC, and SC-ER-EWC methods. These results show that naive SC suffers from severe catastrophic forgetting across tasks and even performs worse than the SB baseline in the CL setting. In contrast, all proposed CL approaches mitigate catastrophic forgetting and yield posterior estimates that are significantly closer to the reference posterior than both naive SC and the SB baseline for most tasks. Among the proposed methods, SC-ER provides the most accurate posterior estimates across all tasks. It effectively prevents catastrophic forgetting while requiring only a single subset per task as a replay buffer, demonstrating that the SC loss can produce accurate posterior estimates with minimal retained data. SC-EWC outperforms naive SC and mitigates forgetting, although its performance remains inferior to SC-ER and only marginally better than SB baseline.

The combined SC-ER-EWC approach likewise mitigates catastrophic forgetting. Its performance is comparable to SC-ER and better than SC-EWC. This suggests that incorporating episodic replay within the self-consistency objective is already sufficient to preserve performance across tasks, and adding the EWC penalty does not provide much additional gains in this setting. Overall, these results highlight the effectiveness of incorporating self-consistency with

lightweight replay mechanisms for robust posterior estimation in CL scenarios. Test-time SC gives accurate posterior estimates when current task inference is the only objective rather than overcoming catastrophic forgetting. Test-time SC prioritizes plasticity (rapid adaptation to the current task) at the expense of stability. In contrast, our CL methods balance plasticity and stability, maintaining performance across all tasks. Additional results including hyperparameter sensitivity analysis for SC-EWC and SC-ER-EWC are provided in Appendix C.

4.2 EXPERIMENT 2: AIR PASSENGER TRAFFIC FORECASTING

Second, we analyze trends in European air passenger traffic data provided by Eurostat [2022a,b,c]. This is a widely used case study in the ABI literature [Habermann et al., 2024, Mishra et al., 2025, Kucharský et al., 2025]. We retrieve time series of annual air passenger counts between 15 European countries (departures) and the USA (destination) from 2004 to 2019. These 15 countries constitute 15 CL tasks. We fit the following auto-regressive process of order 1:

$$y_{j,t+1} \sim \mathcal{N}(\alpha_j + y_{j,t}\beta_j + u_{j,t}\gamma_j + w_{j,t}\delta_j, \sigma_j), \quad (15)$$

where the target quantity $y_{j,t+1}$ is the difference in air passenger traffic for country j between time $t + 1$ and t . To predict $y_{j,t+1}$ we use two additional predictors: $u_{j,t}$ is the annual household debt of country j at time t , measured in % of gross domestic product (GDP) and $w_{j,t}$ is the real GDP per capita. Additional details about the dataset and model are given in Appendix D. We train the neural posterior estimators for all the methods as described in the experimental setup. For episodic replay buffer, we only utilize the data of eight tasks which are chosen based on K-medoid clustering described in Section 2.3.3.

Results In Figure 2, we present the MMD ratio, aggregated over the 15 tasks for naive SC, test-time SC, and the proposed SC-ER, SC-EWC, and SC-ER-EWC methods. Figure 12 in Appendix E depicts the MMD ratio across tasks. Similar to experiment 4.1, naive SC exhibits substantial catastrophic forgetting, whereas the proposed CL approaches effectively mitigate forgetting across tasks. SC-ER provides the most accurate posterior estimates throughout all tasks while maintaining a memory buffer containing data from eight countries for episodic replay. We further investigate the effect of varying the number of tasks retained in the replay buffer which is reported in Figure 13, Appendix E. SC-EWC also overcomes catastrophic forgetting and gives better posterior estimates compared to both naive SC and SB baseline. However, it performs slightly worse than SC-ER.

We observe that SC-ER-EWC performs better than SC-EWC and comparable to SC-ER, indicating that combining ER and EWC can further stabilize learning, though replay

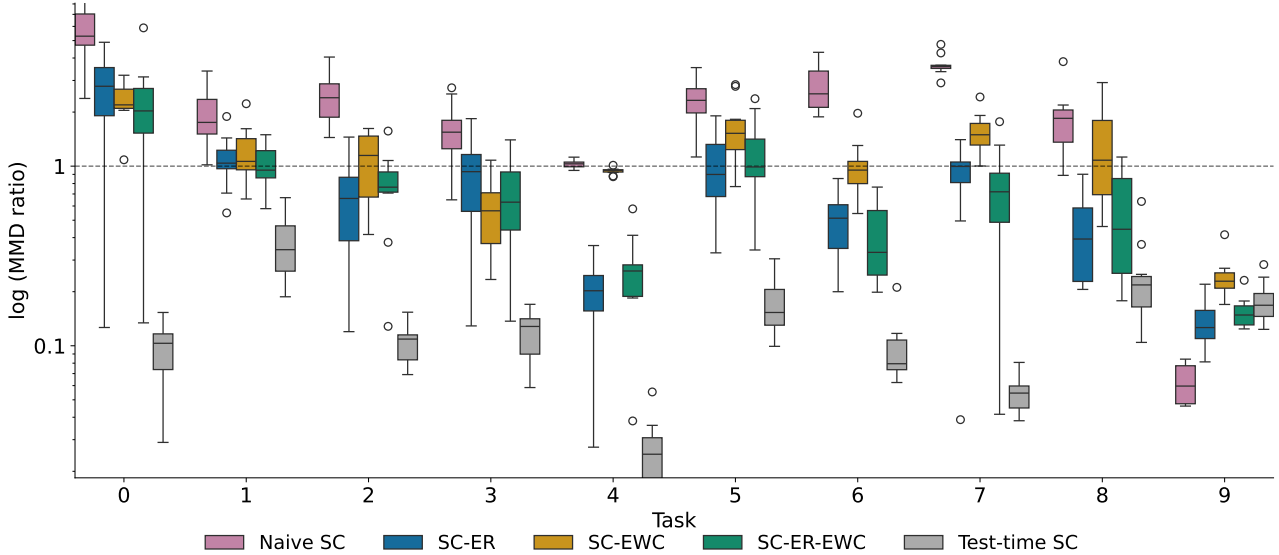


Figure 1: **Experiment 1.** MMD ratio in log scale across CL tasks (0–9) for different methods. Boxes summarize variability across subsets. Dashed line marks parity with simulation-based (SB) baseline (ratio = 1). Naive SC shows catastrophic forgetting in CL setting whereas our proposed methods mitigate forgetting and provide better posterior estimates compared to SB and Naive SC. Test-time SC also gives accurate posterior estimates.

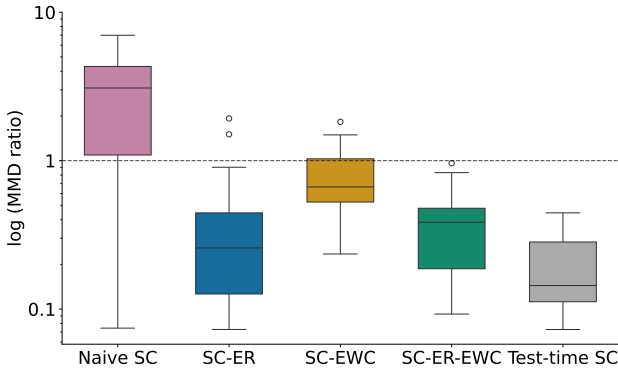


Figure 2: **Experiment 2.** MMD ratio in log scale for different methods aggregated over fifteen CL tasks. Dashed line marks parity with simulation-based baseline (ratio = 1). Naive SC shows catastrophic forgetting in CL setting whereas our proposed methods mitigate forgetting and perform better than both SB baseline and naive SC.

appears to be the dominant contributing factor. We conducted additional experiments varying the size of the replay buffer and observe that the performance of SC-ER-EWC degrades at low memory budget. It nonetheless consistently outperforms both baseline SB and naive SC, as shown in Figure 14, Appendix E. Test-time SC gives accurate posterior estimates when current task inference is the only objective rather than overcoming catastrophic forgetting. However, for most of the tasks, SC-ER performs on par with test-time SC. Additional results are described in Appendix E.

4.3 EXPERIMENT 3: RACING DIFFUSION OF DECISION MAKING

Lastly, we analyze data sets available from a large corpus of experiments on attentional control [Haaf et al., 2025]. From this database, we extracted eight data sets. These eight data sets constitute the eight CL tasks. We further generated one simulated dataset $\{\mathcal{T}_0\}$ of 50 observations from the prior predictive distribution. The data consists of response times (in msec) and response (correct/incorrect).

In this case study, we use the racing diffusion model [RDM, Tillman et al., 2020]. The model assumes that each response is associated with a dedicated noisy evidence accumulator. Each accumulator begins at zero and evolves according to a Wiener process with drift (where W_t is the standard Wiener process),

$$X_t = \nu dt + \sigma dW_t, \quad X_0 = 0. \quad (16)$$

A response is initiated when one of the accumulators first reaches the decision boundary α . The observed response time is the hitting time of the winning accumulator plus a non-decision time τ . The parameters of the model are the decision boundary α , non-decision time τ , and two drift rates ν_1 and ν_2 (associated with correct and incorrect responses, respectively).

We train the neural posterior estimators for all methods as described in the experimental setup. For episodic replay buffer, we retain data from five participant from each previous task – no clustering has been done in this case study. More details about the data, model, and training are in Appendix F.

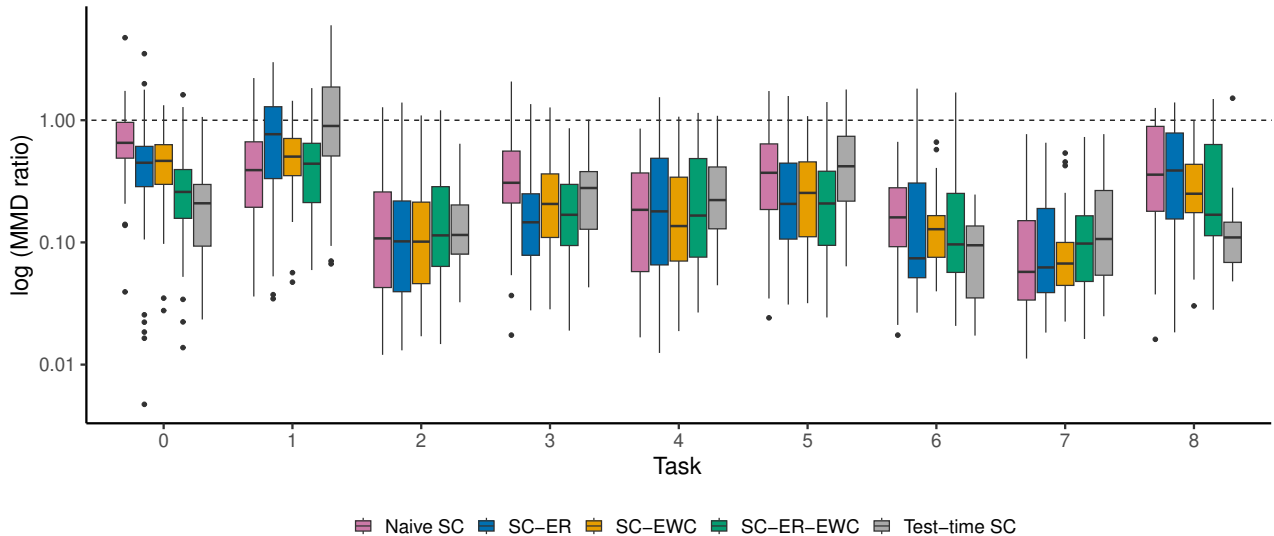


Figure 3: **Experiment 3.** MMD ratio in log scale across CL tasks (0–8) for the four RDM parameters for different methods. Boxes summarize variability over datasets. Dashed line marks parity with simulation-based baseline (ratio = 1). All SC methods outperform SB-only training. Catastrophic forgetting is not evident.

Results Figure 3 shows the MMD ratio across all 9 tasks. In contrast to previous experiments, naive SC does not exhibit pronounced catastrophic forgetting; all methods that utilize any SC training perform clearly better than the SB baseline. Further, CL methods perform on-par even with test-time SC. One possible interpretation of these findings is that the severity of forgetting is dependent on the variability of data within tasks relative to the variability of data between tasks. In the current case study, even though the data sets come from different experiments, they all exhibit similar characteristics: average accuracy ranging between 90%–95% with mean response times between 0.4–0.7 sec. Therefore, it may be the case that the datasets between tasks are similar enough that catastrophic forgetting is not an issue in the first place.

5 DISCUSSION

ABI enables fast posterior inference after simulation-based training, but its accuracy can degrade under distribution shifts. Bayesian self-consistency (SC) losses improve robustness of ABI by leveraging unlabeled empirical data, yet prior work assumes static or single-task setting where all empirical data is readily available. In this work, we adopt a two-stage training procedure consisting of simulation-based pre-training followed by unsupervised self-consistency fine-tuning, to enable network adaptation as new data come in.

We demonstrate that naive application of this procedure can lead to catastrophic forgetting, as network adaptation to a new task can overwrite representations important for earlier tasks, degrading accuracy of the posterior estimates. To ad-

dress this, we introduce more elaborate continual learning mechanisms. Episodic replay (SC-ER) stabilizes learning by retaining a small set of past observations, while elastic weight consolidation (SC-EWC) provides an alternative that constrains parameter updates using importance estimates derived from SC gradients. Across three diverse case studies, both approaches substantially reduce forgetting and yield posterior estimates closer to MCMC reference than simulation-only training and naive SC. The experiments further indicate that the severity of forgetting depends on the degree of distributional variation between tasks. This points to a practical takeaway: when tasks are heterogeneous, replay and/or regularization become important to maintain performance across the full task history.

Limitations and future direction Our self-consistency based continual learning approaches rely on fast density evaluations during training. This makes free-form methods such as flow matching [Lipman et al., 2022] or score-based diffusion [Song et al., 2020] less practical due to their need for numerical integration.

The employed self-consistency losses assume access to the analytic prior and likelihood densities of the probabilistic model. With implicit prior or likelihoods, self-consistency loss is not strictly proper [Mishra et al., 2025] and training with self-consistency has smaller benefits for the accuracy of the posterior approximation [Mishra et al., 2025, Kucharský et al., 2025]. Whether self-consistency or other unsupervised losses can be used effectively in a continual learning setting without access to explicit prior and likelihood densities remains a topic for future research.

Author Contributions

Aayush Mishra and Paul Bürkner conceived the idea. Aayush Mishra developed the methods with the help of Paul Bürkner. Aayush Mishra implemented the first two experiments. Šimon Kucharský implemented the third experiment. Aayush Mishra and Šimon Kucharský drafted the article. All authors contributed to final editing of the article.

Acknowledgements

Paul Bürkner acknowledges support of the DFG Collaborative Research Center 391 (Spatio-Temporal Statistics for the Transition of Energy and Transport) – 520388526.

References

- Richard Abbott, Thomas D Abbott, Fausto Acernese, Kimberly Ackley, Carl Adams, Naresh Adhikari, Radha X Adhikari, Vaishali B Adya, Christoph Affeldt, Deepali Agarwal, et al. Gwtc-3: Compact binary coalescences observed by ligo and virgo during the second part of the third observing run. *Physical Review X*, 13(4):041039, 2023.
- Agil Aghasanli, Yi Li, and Plamen Angelov. Prototype-based continual learning with label-free replay buffer and cluster preservation loss. In *Proceedings of the Computer Vision and Pattern Recognition Conference*, pages 6545–6554, 2025.
- Rahaf Aljundi, Francesca Babiloni, Mohamed Elhoseiny, Marcus Rohrbach, and Tinne Tuytelaars. Memory aware synapses: Learning what (not) to forget. In *Proceedings of the European conference on computer vision (ECCV)*, pages 139–154, 2018.
- Rahaf Aljundi, Klaas Kelchtermans, and Tinne Tuytelaars. Task-free continual learning. In *Proceedings of the IEEE/CVF conference on computer vision and pattern recognition*, pages 11254–11263, 2019.
- James Alvey, Carlo R Contaldi, and Mauro Pironi. Simulation-based inference with deep ensembles: evaluating calibration uncertainty and detecting model misspecification. *Machine Learning: Science and Technology*, 7(1):015008, 2026.
- Patrick Cannon, Daniel Ward, and Sebastian M Schmon. Investigating the impact of model misspecification in neural simulation-based inference. *arXiv preprint arXiv:2209.01845*, 2022.
- Bob Carpenter, Andrew Gelman, Matthew D Hoffman, Daniel Lee, Ben Goodrich, Michael Betancourt, Marcus Brubaker, Jiqiang Guo, Peter Li, and Allen Riddell. Stan: A probabilistic programming language. *Journal of statistical software*, 76:1–32, 2017.
- Arslan Chaudhry, Marcus Rohrbach, Mohamed Elhoseiny, Thalaiyasingam Ajanthan, P Dokania, P Torr, and M Ranzato. Continual learning with tiny episodic memories. In *Workshop on Multi-Task and Lifelong Reinforcement Learning*, 2019.
- Andrey Chetverikov, Polina Iamschinina, Alena Begler, Ivan Ivanchei, Margarita Filippova, and Maria Kuvaldina. Blame everyone: Error-related devaluation in Eriksen flanker task. *Acta Psychologica*, 180:155–159, 2017.
- Michael Deistler, Jan Boelts, Peter Steinbach, Guy Moss, Thomas Moreau, Manuel Gloeckler, Pedro LC Rodrigues, Julia Linhart, Janne K Lappalainen, Benjamin Kurt Miller, et al. Simulation-based inference: A practical guide. *arXiv preprint arXiv:2508.12939*, 2025.
- Charita Dellaporta, Jeremias Knoblauch, Theodoros Damoulas, and François-Xavier Briol. Robust bayesian inference for simulator-based models via the mmd posterior bootstrap. In *International Conference on Artificial Intelligence and Statistics*, pages 943–970. PMLR, 2022.
- Laurent Dinh, Jascha Sohl-Dickstein, and Samy Bengio. Density estimation using real nvp. *arXiv preprint arXiv:1605.08803*, 2016.
- Conor Durkan, Artur Bekasov, Iain Murray, and George Papamakarios. Neural spline flows. *Advances in neural information processing systems*, 32, 2019.
- Lasse Elsemüller, Hans Olischläger, Marvin Schmitt, Paul-Christian Bürkner, Ullrich Köthe, and Stefan T Radev. Sensitivity-aware amortized bayesian inference. *arXiv preprint arXiv:2310.11122*, 2023.
- Lasse Elsemüller, Valentin Pratz, Mischa von Krause, Andreas Voss, Paul-Christian Bürkner, and Stefan T Radev. Does unsupervised domain adaptation improve the robustness of amortized bayesian inference? a systematic evaluation. *arXiv preprint arXiv:2502.04949*, 2025.
- Barbara A Eriksen and Charles W Eriksen. Effects of noise letters upon the identification of a target letter in a non-search task. *Perception & psychophysics*, 16(1):143–149, 1974.
- Eurostat. International extra-eu air passenger transport by reporting country and partner world regions and countries, doi:10.2908/avia_paexcc, 2022a.
- Eurostat. Household debt, consolidated including Non-profit institutions serving households - % of GDP, doi:10.2908/TIPSD22, 2022b.
- Eurostat. Real gdp per capita, doi:10.2908/SDG_08_10, 2022c.

- Matthias Feurer, Jan N. van Rijn, Arind Kadra, Pieter Gijsbers, Neeratyoy Mallik, Sahithya Ravi, Andreas Müller, Joaquin Vanschoren, and Frank Hutter. Openml-python: an extensible python api for openml. *Journal of Machine Learning Research*, 22(100):1–5, 2021. URL <http://jmlr.org/papers/v22/19-920.html>.
- David T Frazier, Ryan Kelly, Christopher Drovandi, and David J Warne. The statistical accuracy of neural posterior and likelihood estimation. *arXiv preprint arXiv:2411.12068*, 2024.
- Aritra Ghosh, C Megan Urry, Aayush Mishra, Laurence Perreault-Levasseur, Priyamvada Natarajan, David B Sanders, Daisuke Nagai, Chuan Tian, Nico Cappelluti, Jeyhan S Kartaltepe, et al. Morphological parameters and associated uncertainties for 8 million galaxies in the hyper supprime-cam wide survey. *The Astrophysical Journal*, 953(2):134, 2023.
- Manuel Gloeckler, Michael Deistler, and Jakob H Macke. Adversarial robustness of amortized bayesian inference. *arXiv preprint arXiv:2305.14984*, 2023.
- Manuel Gloeckler, Michael Deistler, Christian Weibach, Frank Wood, and Jakob H Macke. All-in-one simulation-based inference. *arXiv preprint arXiv:2404.09636*, 2024.
- Alex Gomez-Villa, Bartłomiej Twardowski, Kai Wang, and Joost Van de Weijer. Plasticity-optimized complementary networks for unsupervised continual learning. In *Proceedings of the IEEE/CVF winter conference on applications of computer vision*, pages 1690–1700, 2024.
- Arthur Gretton, Karsten M Borgwardt, Malte J Rasch, Bernhard Schölkopf, and Alexander Smola. A kernel two-sample test. *The journal of machine learning research*, 13(1):723–773, 2012.
- Julia M Haaf, Madlen Hoffstadt, and Sven Lesche. Attentional control data collection: A resource for efficient data reuse. *Behavior Research Methods*, 57(8):208, 2025.
- Daniel Habermann, Marvin Schmitt, Lars Kühmichel, Andreas Bulling, Stefan T Radev, and Paul-Christian Bürkner. Amortized bayesian multilevel models. *arXiv preprint arXiv:2408.13230*, 2024.
- Kam Hamidieh. A data-driven statistical model for predicting the critical temperature of a superconductor. *Computational Materials Science*, 154:346–354, 2018.
- David Harrison Jr and Daniel L Rubinfeld. Hedonic housing prices and the demand for clean air. *Journal of environmental economics and management*, 5(1):81–102, 1978.
- Craig Hedge, Georgina Powell, and Petroc Sumner. The reliability paradox: Why robust cognitive tasks do not produce reliable individual differences. *Behavior research methods*, 50(3):1166–1186, 2018.
- Daolang Huang, Ayush Bharti, Amauri Souza, Luigi Acerbi, and Samuel Kaski. Learning robust statistics for simulation-based inference under model misspecification. *Advances in Neural Information Processing Systems*, 36:7289–7310, 2023.
- Leonard Kaufman and Peter J Rousseeuw. *Finding groups in data: an introduction to cluster analysis*. John Wiley & Sons, 2009.
- James Kirkpatrick, Razvan Pascanu, Neil Rabinowitz, Joel Veness, Guillaume Desjardins, Andrei A Rusu, Kieran Milan, John Quan, Tiago Ramalho, Agnieszka Grabska-Barwinska, et al. Overcoming catastrophic forgetting in neural networks. *Proceedings of the national academy of sciences*, 114(13):3521–3526, 2017.
- Ivan Kobyzev, Simon JD Prince, and Marcus A Brubaker. Normalizing flows: An introduction and review of current methods. *IEEE transactions on pattern analysis and machine intelligence*, 43(11):3964–3979, 2020.
- Ullrich Köthe. A review of change of variable formulas for generative modeling. *arXiv preprint arXiv:2308.02652*, 2023.
- Jędrzej Kozal, Jan Wasilewski, Bartosz Krawczyk, and Michał Woźniak. Continual learning with weight interpolation. In *Proceedings of the IEEE/CVF conference on computer vision and pattern recognition*, pages 4187–4195, 2024.
- Šimon Kucharský, Aayush Mishra, Daniel Habermann, Stefan T. Radev, and Paul-Christian Bürkner. Improving the Accuracy of Amortized Model Comparison with Self-Consistency. *arXiv preprint*, 2025. doi: 10.48550/arXiv.2508.20614.
- Lars Kühmichel, Jerry M Huang, Valentin Pratz, Jonas Arruda, Hans Olischläger, Daniel Habermann, Simon Kucharsky, Lasse Elsemüller, Aayush Mishra, Niels Bracher, et al. Bayesflow 2.0: Multi-backend amortized bayesian inference in python. *arXiv preprint arXiv:2602.07098*, 2026.
- Juho Lee, Yoonho Lee, Jungtaek Kim, Adam Kosiorek, Seungjin Choi, and Yee Whye Teh. Set transformer: A framework for attention-based permutation-invariant neural networks. In *International conference on machine learning*, pages 3744–3753. PMLR, 2019a.
- Kimin Lee, Sukmin Yun, Kibok Lee, Honglak Lee, Bo Li, and Jinwoo Shin. Robust inference via generative classifiers for handling noisy labels. In *International conference on machine learning*, pages 3763–3772. PMLR, 2019b.
- Alex Lewandowski, Michał Bortkiewicz, Saurabh Kumar, András György, Dale Schuurmans, Mateusz Ostaszewski,

- and Marlos C Machado. Learning continually by spectral regularization. In *The Thirteenth International Conference on Learning Representations*. OpenReview. net, 2025.
- Xingyu Li, Bo Tang, and Haifeng Li. Adaer: An adaptive experience replay approach for continual lifelong learning. *Neurocomputing*, 572:127204, 2024.
- Zhizhong Li and Derek Hoiem. Learning without forgetting. *IEEE transactions on pattern analysis and machine intelligence*, 40(12):2935–2947, 2017.
- Yaron Lipman, Ricky TQ Chen, Heli Ben-Hamu, Maximilian Nickel, and Matt Le. Flow matching for generative modeling. *arXiv preprint arXiv:2210.02747*, 2022.
- Aojun Lu, Tao Feng, Hangjie Yuan, Xiaotian Song, and Yanan Sun. Revisiting neural networks for continual learning: An architectural perspective. *arXiv preprint arXiv:2404.14829*, 2024.
- Divyam Madaan, Jaehong Yoon, Yuanchun Li, Yunxin Liu, and Sung Ju Hwang. Representational continuity for unsupervised continual learning. *arXiv preprint arXiv:2110.06976*, 2021.
- Kolby Nottingham Markelle Kelly, Rachel Longjohn. The uci machine learning repository. <https://archive.ics.uci.edu>.
- Aayush Mishra, Daniel Habermann, Marvin Schmitt, Stefan T Radev, and Paul-Christian Bürkner. Robust amortized bayesian inference with self-consistency losses on unlabeled data. *arXiv preprint arXiv:2501.13483*, 2025.
- Diganta Misra. Mish: A self regularized non-monotonic activation function. *arXiv preprint arXiv:1908.08681*, 2019.
- R Kelley Pace and Ronald Barry. Sparse spatial autoregressions. *Statistics & Probability Letters*, 33(3):291–297, 1997.
- George Papamakarios, Eric Nalisnick, Danilo Jimenez Rezende, Shakir Mohamed, and Balaji Lakshminarayanan. Normalizing flows for probabilistic modeling and inference. *Journal of Machine Learning Research*, 22(57):1–64, 2021.
- German I Parisi, Ronald Kemker, Jose L Part, Christopher Kanan, and Stefan Wermter. Continual lifelong learning with neural networks: A review. *Neural networks*, 113: 54–71, 2019.
- Fabian Pedregosa, Gaël Varoquaux, Alexandre Gramfort, Vincent Michel, Bertrand Thirion, Olivier Grisel, Mathieu Blondel, Peter Prettenhofer, Ron Weiss, Vincent Dubourg, et al. Scikit-learn: Machine learning in python. *the Journal of machine Learning research*, 12:2825–2830, 2011.
- Michael S Pratte, Jeffrey N Rouder, Richard D Morey, and Chuning Feng. Exploring the differences in distributional properties between Stroop and Simon effects using delta plots. *Attention, Perception, & Psychophysics*, 72(7): 2013–2025, 2010.
- Stefan T Radev, Marvin Schmitt, Lukas Schumacher, Lasse Elsemüller, Valentin Pratz, Yannik Schälte, Ullrich Köthe, and Paul-Christian Bürkner. Bayesflow: Amortized bayesian workflows with neural networks. *arXiv preprint arXiv:2306.16015*, 2023.
- Dushyant Rao, Francesco Visin, Andrei Rusu, Razvan Pascanu, Yee Whye Teh, and Raia Hadsell. Continual unsupervised representation learning. *Advances in neural information processing systems*, 32, 2019.
- Lorenz Richter and Julius Berner. Improved sampling via learned diffusions. *arXiv preprint arXiv:2307.01198*, 2023.
- Lorenz Richter, Ayman Boustati, Nikolas Nüsken, Francisco Ruiz, and Omer Deniz Akyildiz. Vargrad: a low-variance gradient estimator for variational inference. *Advances in Neural Information Processing Systems*, 33:13481–13492, 2020.
- David Rolnick, Arun Ahuja, Jonathan Schwarz, Timothy Lillicrap, and Gregory Wayne. Experience replay for continual learning. *Advances in neural information processing systems*, 32, 2019.
- Andrei A Rusu, Neil C Rabinowitz, Guillaume Desjardins, Hubert Soyer, James Kirkpatrick, Koray Kavukcuoglu, Razvan Pascanu, and Raia Hadsell. Progressive neural networks. *arXiv preprint arXiv:1606.04671*, 2016.
- Sebastian Sanokowski, Lukas Gruber, Christoph Bartmann, Sepp Hochreiter, and Sebastian Lehner. Rethinking losses for diffusion bridge samplers. *arXiv preprint arXiv:2506.10982*, 2025.
- Marvin Schmitt, Paul-Christian Bürkner, Ullrich Köthe, and Stefan T Radev. Detecting model misspecification in amortized bayesian inference with neural networks. In *Dagm german conference on pattern recognition*, pages 541–557. Springer, 2023a.
- Marvin Schmitt, Desi R Ivanova, Daniel Habermann, Ullrich Köthe, Paul-Christian Bürkner, and Stefan T Radev. Leveraging self-consistency for data-efficient amortized bayesian inference. *arXiv preprint arXiv:2310.04395*, 2023b.
- Jonathan Schwarz, Wojciech Czarnecki, Jelena Luketina, Agnieszka Grabska-Barwinska, Yee Whye Teh, Razvan Pascanu, and Raia Hadsell. Progress & compress: A scalable framework for continual learning. In *International conference on machine learning*, pages 4528–4537. PMLR, 2018.

- Hanul Shin, Jung Kwon Lee, Jaehong Kim, and Jiwon Kim. Continual learning with deep generative replay. *Advances in neural information processing systems*, 30, 2017.
- J Richard Simon. The effects of an irrelevant directional cue on human information processing. In *Advances in psychology*, volume 65, pages 31–86. Elsevier, 1990.
- Jiaming Song, Chenlin Meng, and Stefano Ermon. Denoising diffusion implicit models. *arXiv preprint arXiv:2010.02502*, 2020.
- J Ridley Stroop. Studies of interference in serial verbal reactions. *Journal of experimental psychology*, 18(6):643, 1935.
- Chuan Tian, C Megan Urry, Aritra Ghosh, Daisuke Nagai, Tonima T Ananna, Meredith C Powell, Connor Auge, Aayush Mishra, David B Sanders, Nico Cappelluti, et al. Automatic machine learning framework to study morphological parameters of agn host galaxies within $z < 1.4$ in the hyper supreme-cam wide survey. *The Astrophysical Journal*, 981(1):5, 2025.
- Gabriel Tillman, Trish Van Zandt, and Gordon D Logan. Sequential sampling models without random between-trial variability: The racing diffusion model of speeded decision making. *Psychonomic Bulletin & Review*, 27(5): 911–936, 2020.
- Ruilin Tong, Haodong Lu, Yuhang Liu, and Dong Gong. Model inversion with layer-specific modeling and alignment for data-free continual learning. *arXiv preprint arXiv:2510.26311*, 2025.
- Gido M Van de Ven and Andreas S Tolias. Three scenarios for continual learning. *arXiv preprint arXiv:1904.07734*, 2019.
- Liyuan Wang, Xingxing Zhang, Hang Su, and Jun Zhu. A comprehensive survey of continual learning: Theory, method and application. *IEEE transactions on pattern analysis and machine intelligence*, 46(8):5362–5383, 2024.
- Daniel Ward, Patrick Cannon, Mark Beaumont, Matteo Fasiolo, and Sebastian Schmon. Robust neural posterior estimation and statistical model criticism. *Advances in Neural Information Processing Systems*, 35:33845–33859, 2022.
- Antoine Wehenkel, Juan L Gamella, Ozan Sener, Jens Behrmann, Guillermo Sapiro, Jörn-Henrik Jacobsen, and Marco Cuturi. Addressing misspecification in simulation-based inference through data-driven calibration. *arXiv preprint arXiv:2405.08719*, 2024.
- Jonas Wildberger, Maximilian Dax, Simon Buchholz, Stephen Green, Jakob H Macke, and Bernhard Schölkopf. Flow matching for scalable simulation-based inference. *Advances in Neural Information Processing Systems*, 36: 16837–16864, 2023.
- Xinyao Wu, Zhe Xu, and Raymond Kai-yu Tong. Continual learning in medical image analysis: A survey. *Computers in Biology and Medicine*, 182:109206, 2024.
- Jason Yoo, Yunpeng Liu, Frank Wood, and Geoff Pleiss. Layerwise proximal replay: A proximal point method for online continual learning. *arXiv preprint arXiv:2402.09542*, 2024.
- Manzil Zaheer, Satwik Kottur, Siamak Ravanbakhsh, Barnabas Poczos, Russ R Salakhutdinov, and Alexander J Smola. Deep sets. *Advances in neural information processing systems*, 30, 2017.
- Andrew Zammit-Mangion, Matthew Sainsbury-Dale, and Raphaël Huser. Neural methods for amortized inference. *Annual Review of Statistics and Its Application*, 12(1): 311–335, 2025.
- Friedemann Zenke, Ben Poole, and Surya Ganguli. Continual learning through synaptic intelligence. In *International conference on machine learning*, pages 3987–3995. PMLR, 2017.
- Xuyang Zhao, Huiyuan Wang, Weiran Huang, and Wei Lin. A statistical theory of regularization-based continual learning. In *International Conference on Machine Learning*, pages 61021–61039. PMLR, 2024.

Unsupervised CL for Amortized Bayesian Inference (Supplementary Material)

Aayush Mishra¹

Šimon Kucharský¹

Paul-Christian Bürkner¹

¹Department of Statistics, TU Dortmund University, Germany

A ADDITIONAL ALGORITHMS

Algorithm 3 Self-Consistency with Episodic Replay and Elastic Weight Consolidation

- 1: **Input:** Simulated dataset $(\theta, x) \sim p(\theta, x)$, unlabeled tasks $\{\mathcal{T}_t\}_{t=1}^T$, EWC weight λ , Fisher batches B , replay size K
 - 2: **Output:** Posterior estimator $q_\Phi(\theta | x)$
 - 3: Initialize q_Φ , replay buffer $\mathcal{E} \leftarrow \emptyset$, EWC record list $\mathcal{R} \leftarrow \emptyset$
 - 4: **Simulation-based pre-training**
 - 5: **for** pretraining iterations **do**
 - 6: Sample $(\theta, x) \sim p(\theta, x)$
 - 7: Update Φ by minimizing \mathcal{L}_{SB} from Eq. 3
 - 8: **end for**
 - 9: **CL**
 - 10: **for** $t = 1$ to T **do**
 - 11: Obtain current dataset $x_t^* \sim p_t^*(x)$ from task \mathcal{T}_t
 - 12: Concatenate replay data with current data:
 $x_{SC}^* \leftarrow x_t^* \cup \mathcal{E}$
 - 13: **for** each SC-ER-EWC iteration **do**
 - 14: **if** $\mathcal{R} \neq \emptyset$ and $\mathcal{E} \neq \emptyset$ **then**
 - 15: Update q_Φ by minimizing $\mathcal{L}_{SC-ER-EWC}$ from Eq. 12
 - 16: **else**
 - 17: Update q_Φ by minimizing \mathcal{L}_{SC} from Eq. 5
 - 18: **end if**
 - 19: **end for**
 - 20: **if** using clustering **then**
 - 21: Draw posterior samples $\{\theta_t^{(s)}\}$ from $q_\Phi(\theta | x_t^*)$
 - 22: $\mathcal{E} \leftarrow \text{KMEDOIDUPDATE}(\mathcal{E}, x_t^*, \{\theta_t^{(s)}\})$
 - 23: **else**
 - 24: Store a subset of data from \mathcal{T}_t in \mathcal{E}
 - 25: **end if**
 - 26: Estimate $\mathcal{W}_{jj}^{(t)}$ for task \mathcal{T}_t as per Eq. 10
 - 27: Snapshot parameters Φ_t^*
 - 28: Append $(\Phi_t^*, \mathcal{W}_{jj}^{(t)})$ to EWC record list \mathcal{R}
 - 29: **end for**
 - 30: **Return** $q_\Phi(\theta | x)$
-

Algorithm 4 KMEDOIDUPDATE

```
1: Input: Current memory  $\mathcal{E}$ , new task  $x_t^*$ , posterior samples  $\{\theta_t^{(s)}\}$ , memory size  $K$ 
2: Output: Updated memory  $\mathcal{E}$ 
3: Add  $(x_t^*, \{\theta_t^{(s)}\})$  to  $\mathcal{E}$ 
4: if  $|\mathcal{E}| \leq K$  then
5:   return  $\mathcal{E}$ 
6: else
7:   Form posterior representations  $\{\bar{\theta}_i\}$ 
8:   Apply K-medoids clustering in parameter space and let  $\mathcal{M}$  be the set of indices of cluster representatives
9:   Retain only cluster representatives and discard the rest ( $\mathcal{E} \leftarrow \{(x_i^*, \{\theta_i^{(s)}\}) : i \in \mathcal{M}\}$ )
10:  return  $\mathcal{E}$ 
11: end if
```

B EXPERIMENT 1: DATASET AND MODEL DESCRIPTION

For continual learning, we utilize nine real-world regression datasets, each treated as a sequential task in the CL setting (Tasks 1–9). For each dataset, we select five representative predictors and consider a single continuous response variable. The datasets are obtained from standard public repositories, including OpenML [Feurer et al., 2021], scikit-learn [Pedregosa et al., 2011], and the UCI Machine Learning Repository [Markelle Kelly].

Task 1: Boston Housing. We use the Boston Housing dataset [Harrison Jr and Rubinfeld, 1978] from OpenML (version 1). Predictors: CRIM (crime rate), ZN (residential land proportion), RM (average number of rooms), AGE (proportion of old units), and DIS (distance to employment centers). Response: Median house value.

Task 2: Auto MPG. We use the Auto MPG dataset from OpenML (version 1). Predictors: cylinders, displacement, horsepower, weight, and acceleration. Response: Miles per gallon (mpg), a continuous measure of fuel efficiency.

Task 3: California Housing. We use the California Housing dataset [Pace and Barry, 1997] from scikit-learn. Predictors: MedInc (median income), HouseAge, AveRooms, AveOccup, and Population. Response: Median house value.

Task 4: Diabetes. We use the Diabetes dataset from scikit-learn. Predictors: bmi (body mass index), bp (blood pressure), s1 and s5 (serum measurements), and age. Response: Quantitative measure of disease progression one year after baseline.

Task 5: Energy Efficiency. We use the Energy Efficiency dataset (UCI ID 242). Predictors: Relative Compactness (X1), Surface Area (X3), Wall Area (X6), Overall Height (X7), and Glazing Area (X8). Response: Heating Load (Y1).

Task 6: Bike Sharing. We use the Bike Sharing dataset (UCI ID 275). Predictors: mnth (month), temp (temperature), hum (humidity), windspeed, and weekday. Response: Bike rental count.

Task 7: Concrete Compressive Strength. We use the Concrete Compressive Strength dataset (UCI ID 165). Predictors: Cement, Water, Superplasticizer, Coarse Aggregate, and Fly Ash. Response: Concrete compressive strength.

Task 8: Liver Disorders. We use the Liver Disorders dataset (UCI ID 60). Predictors: mcv, alkphos, sgpt, sgot, and gammagt (blood test measurements). Response: Continuous liver disorder indicator.

Task 9: Superconductivity. We use the Superconductivity dataset (UCI ID 464) [Hamidieh, 2018]. Predictors: mean_atomic_mass, mean_Valence, mean_atomic_radius, mean_ElectronAffinity, and mean_FusionHeat. Response: Critical temperature of superconducting materials.

Across all tasks, input features are standardized prior to training. The dataset for Task 0 was simulated from the prior predictive distribution. For each task, we partition the data into 10 subsets with 100 observations each. The observations were sampled independently from the full dataset with replacement.

For the summary network, we use set-transformer [Lee et al., 2019a] an attention-based permutation-invariant neural network to learn 50-dimensional embeddings that are maximally informative for posterior inference. For the neural posterior

estimator $q(\theta | x)$, we use a neural spline flow [Durkan et al., 2019] with 6 coupling layers of 128 units each utilizing exponential linear unit activation functions and a multivariate unit Gaussian latent space. These settings were the same for both the standard simulation-based pre-training and for the training of unsupervised CL methods.

The posterior network and summary networks are jointly trained. For SB baseline, we use online training with 64 simulation batches and a batch size of 32 for 50 epochs with a learning rate of 10^{-3} . For subsequent unsupervised training of naive SC, SC-ER, SC-EWC, SC-ER-EWC, and test-time SC, we use the Adam optimizer with a cosine decay learning rate schedule. The initial learning rate is initialized as $10^{-3} \cdot t$, where t is the task index, and is annealed following a cosine schedule over all training steps. Training is done for 30 epochs for each task with each step utilizing the entire data set for computing the SC loss, with the variance target computed over 16 samples from the current posterior approximation [Mishra et al., 2025].

C EXPERIMENT 1: ADDITIONAL RESULTS

We conducted a sensitivity analysis to evaluate the effect of the EWC regularization strength parameter, λ , which controls the degree of constraint imposed on previously learned parameters. Specifically, we trained both SC-EWC and SC-ER-EWC with λ values ranging from 10^2 to 10^5 , while keeping all other hyperparameters fixed. The corresponding MMD ratio values across tasks are reported in Figures 4 and 5 for SC-EWC and SC-ER-EWC, respectively.

For SC-EWC, we observe that the variant with $\lambda = 10^2$ exhibits noticeably stronger catastrophic forgetting on several tasks compared to configurations with larger λ values. Increasing the regularization strength mitigates this effect, and overall performance remains relatively stable for $\lambda \in 10^3, 10^4, 10^5$, with $\lambda = 10^3$ yielding the best performance across tasks.

In contrast, for SC-ER-EWC, performance remains largely stable even for smaller λ values, indicating that the robustness improvements are primarily attributable to episodic replay. The addition of EWC provides only marginal benefits in this setting. However, when λ is increased to 10^5 , performance deteriorates relative to other configurations, suggesting that overly strong regularization can hinder adaptation and negatively impact robustness.

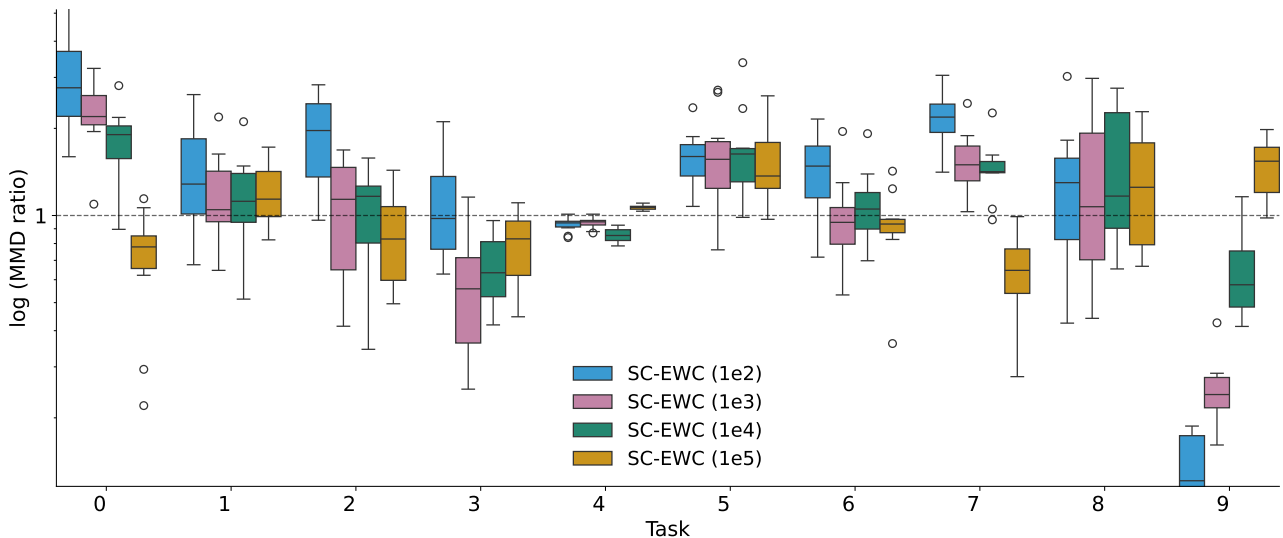


Figure 4: **Experiment 1.** MMD ratio in log scale across CL tasks (0–9) for SC-EWC with different values of EWC hyperparameter λ . Boxes summarize variability across subsets. Dashed line marks parity with simulation-based (SB) baseline (ratio = 1). $\lambda = 10^2$ shows forgetting while other variants perform similarly.

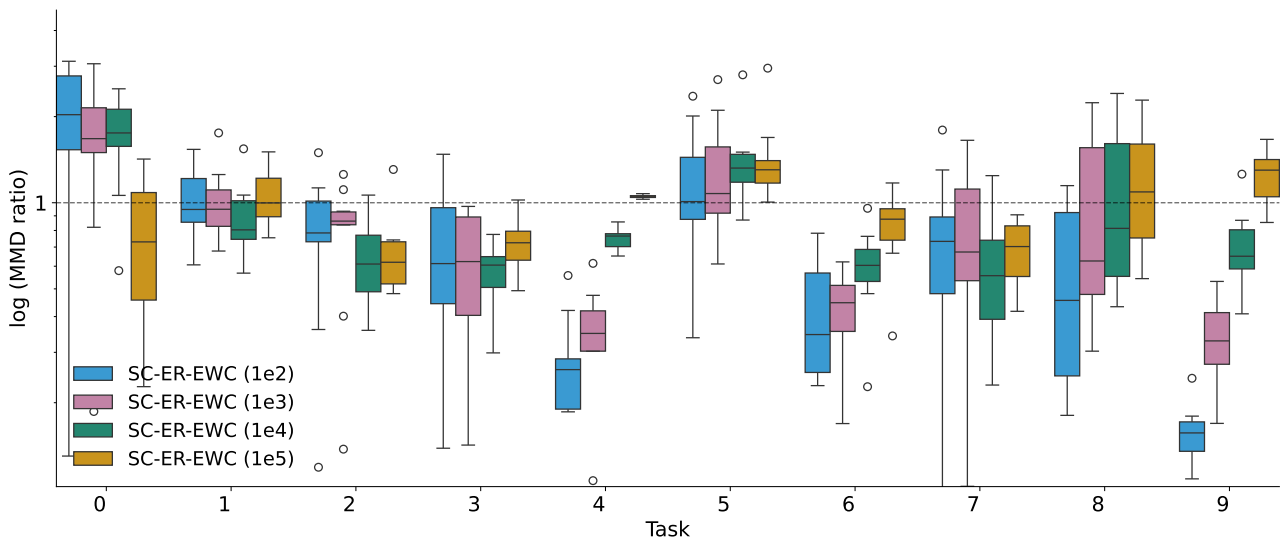


Figure 5: **Experiment 1.** MMD ratio in log scale across CL tasks (0–9) for SC-ER-EWC with different values of EWC hyperparameter λ . Boxes summarize variability across subsets. Dashed line marks parity with simulation-based (SB) baseline (ratio = 1). The performance remains largely stable even for smaller λ values, indicating that the robustness improvements are primarily attributable to episodic replay. The addition of EWC provides only marginal benefits in this setting.

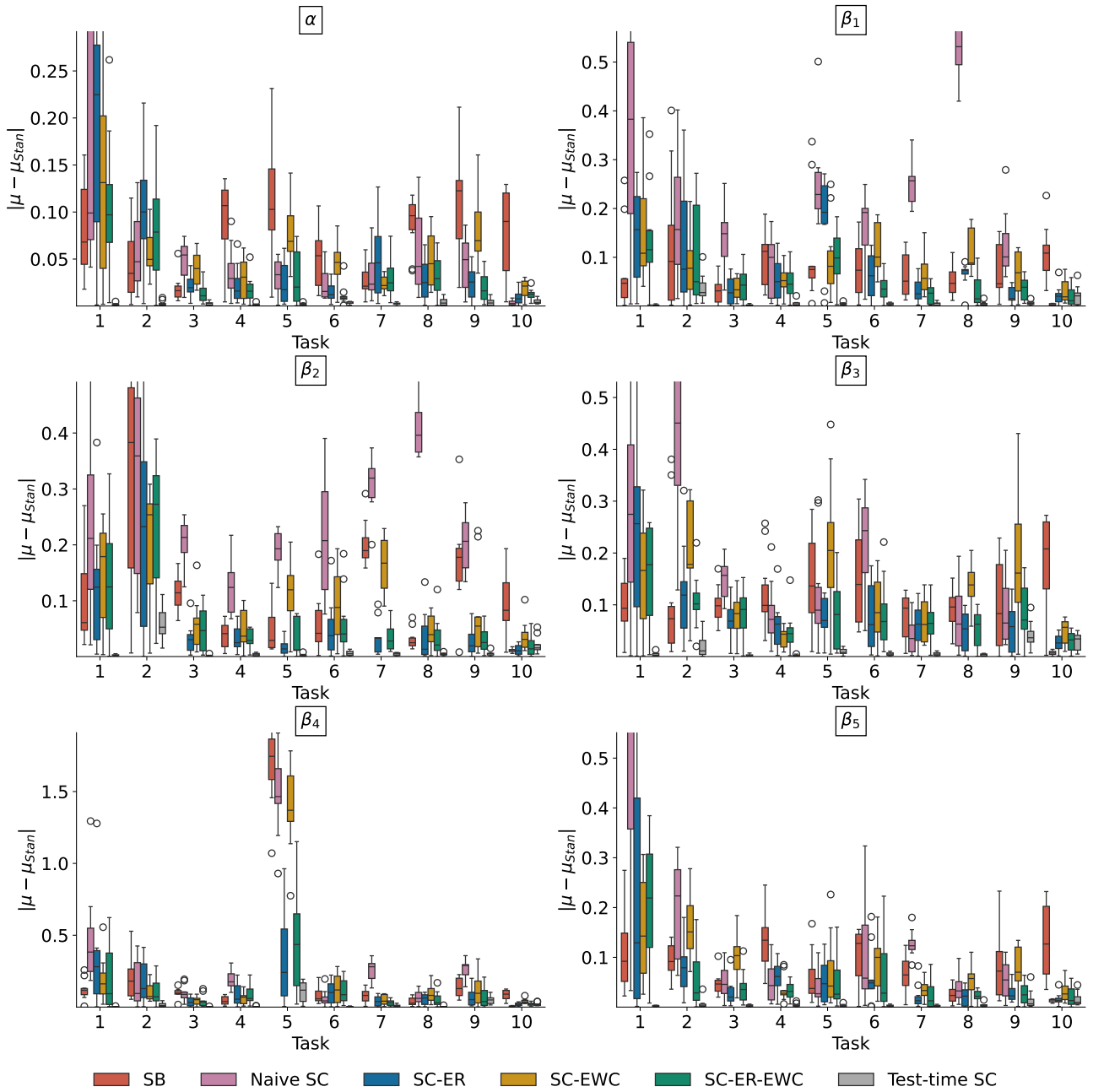


Figure 6: **Experiment 1.** Absolute mean bias of linear regression parameters compared to Stan based estimates across CL tasks (0–9) for various methods. Boxes summarize variability across subsets. SB and naive SC show catastrophic forgetting while CL methods perform consistently better across tasks.

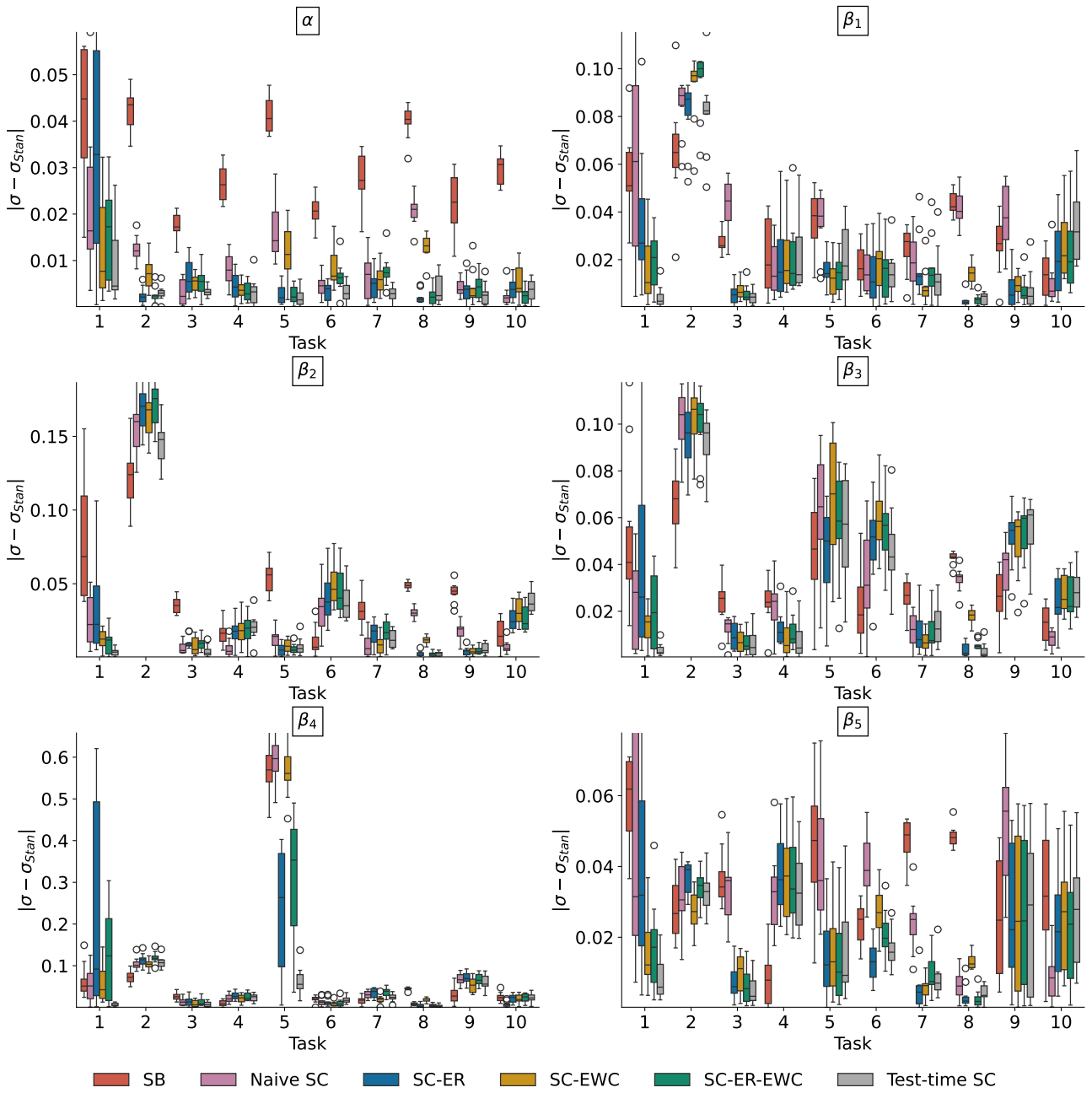


Figure 7: **Experiment 1.** Absolute standard deviation bias of linear regression parameters compared to Stan based estimates across CL tasks (0–9) for various methods. Boxes summarize variability across subsets.

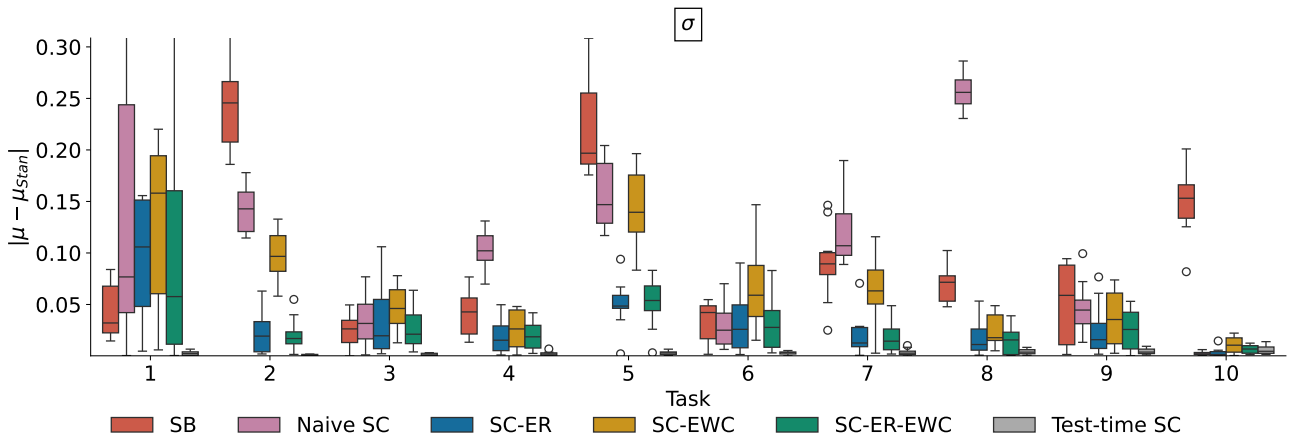


Figure 8: **Experiment 1.** Absolute mean bias of linear regression parameter σ compared to Stan based estimates across CL tasks (0–9) for various methods. Boxes summarize variability across subsets. SB and naive SC show high bias across tasks while other methods perform consistently better.

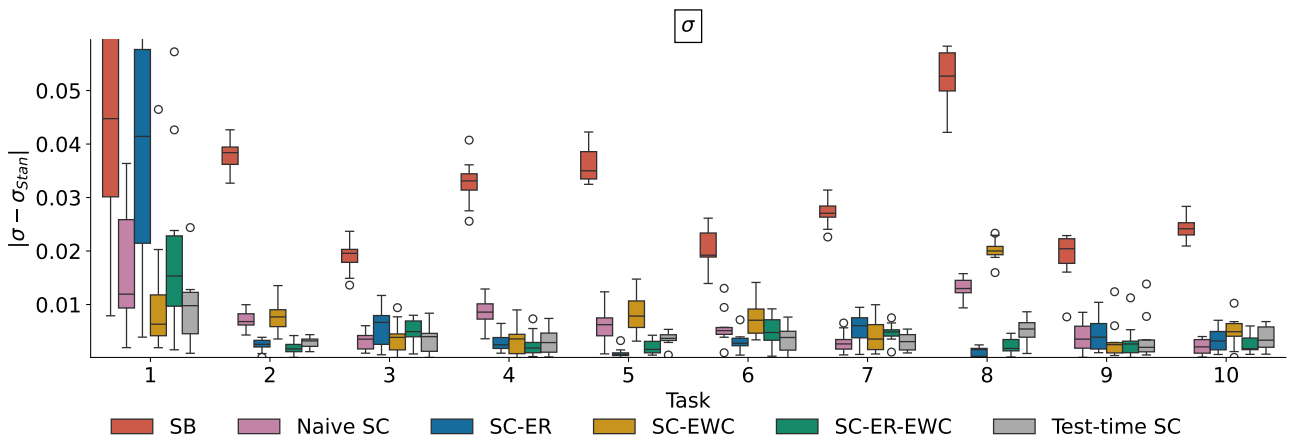


Figure 9: **Experiment 1.** Absolute standard deviation bias of linear regression parameter σ compared to Stan based estimates across CL tasks (0–9) for various methods. Boxes summarize variability across subsets. SB shows high bias across tasks while other methods perform consistently better.

D EXPERIMENT 2: DATASET AND MODEL DESCRIPTION

The parameters α_j denote country-level intercepts, β_j are the autoregressive coefficients, γ_j are the regression coefficients of household debt and δ_j are the regression coefficients of GDP per capita, and σ_j is the standard deviation of the noise term. This model has previously been applied within ABI in Habermann et al. [2024], Mishra et al. [2025], Kucharský et al. [2025]. Following standard practice for autoregressive models, we regress on time period differences to mitigate non-stationarity. This is critical for simulation-based inference because $\beta_j > 1$ can induce exponential growth and quickly produce unrealistic air traffic volumes. Moreover, amortizing over covariate spaces, such as varying GDP per capita between countries, can lead to model misspecification if such fluctuations are underrepresented in training.

For the air traffic model defined in Section 4.2, we set independent priors on the parameters as follows:

$$\begin{aligned} \alpha_j &\sim \mathcal{N}(0, 0.5) & \beta_j &\sim \mathcal{N}(0, 0.2) \\ \gamma_j &\sim \mathcal{N}(0, 0.5) & \delta_j &\sim \mathcal{N}(0, 0.5) \\ \log(\sigma_j) &\sim \mathcal{N}(-1, 0.5). \end{aligned}$$

For the summary network, we use a long short-term memory layer with 64 output dimensions followed by two dense layers with output dimensions of 256 and 64. For the neural posterior estimator $q(\theta | x)$, we use a neural spline flow [Durkan et al., 2019] with 6 coupling layers of 128 units each utilizing exponential linear unit activation functions and a multivariate unit Gaussian latent space. These settings were the same for both the standard simulation-based pre-training and for the training of unsupervised CL methods.

The posterior network and summary networks are jointly trained. For SB baseline, we use online training with 64 simulation batches and a batch size of 32 for 50 epochs with a learning rate of 10^{-3} . For subsequent unsupervised training of naive SC, SC-ER, SC-EWC, SC-ER-EWC, and test-time SC, we use the Adam optimizer with a cosine decay learning rate schedule. The initial learning rate is initialized as $10^{-3} \cdot t$, where t is the task index, and is annealed following a cosine schedule over all training steps. Training is done for 30 epochs for each task with each step utilizing the entire data set for computing the SC loss, with the variance target computed over 16 samples from the current posterior approximation [Mishra et al., 2025].

E EXPERIMENT 2: ADDITIONAL RESULTS

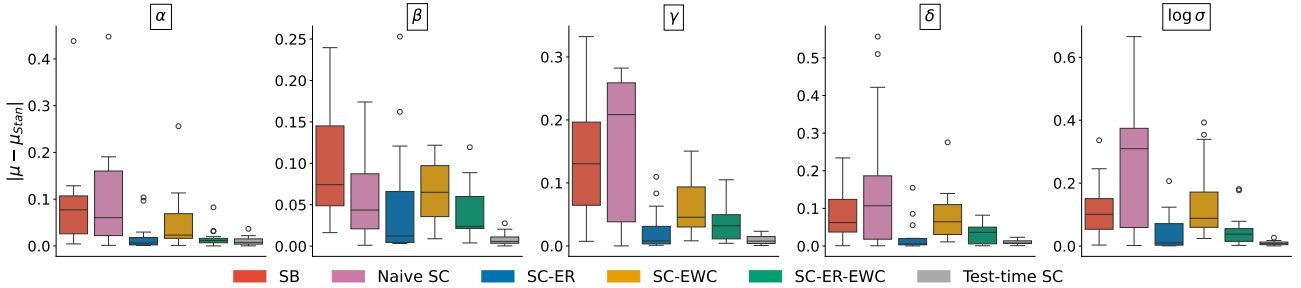


Figure 10: **Experiment 2.** Absolute mean bias of air traffic model parameters compared to Stan based estimates for various methods aggregated over 15 CL tasks. Boxes summarize variability of parameters across tasks. SB and naive SC show high bias across tasks while other methods perform consistently better.

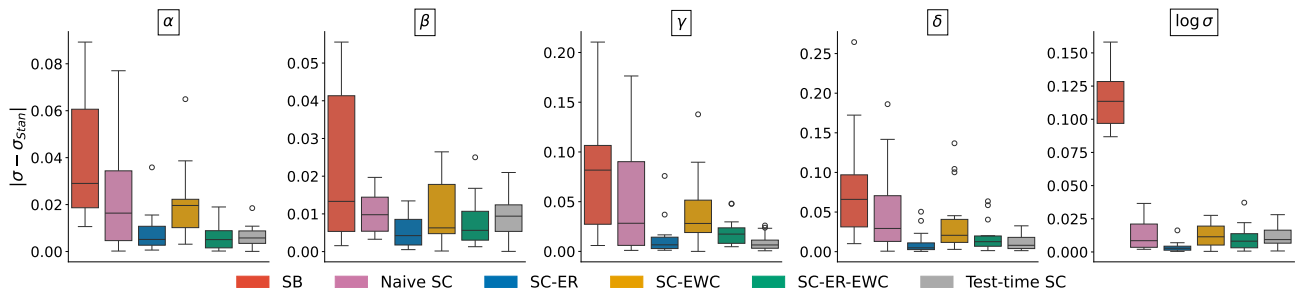


Figure 11: **Experiment 2.** Absolute standard deviation bias of air traffic model parameters compared to Stan based estimates for various methods aggregated over 15 CL tasks. Boxes summarize variability of parameters across tasks. SB and naive SC show high bias across tasks while other methods perform consistently better.

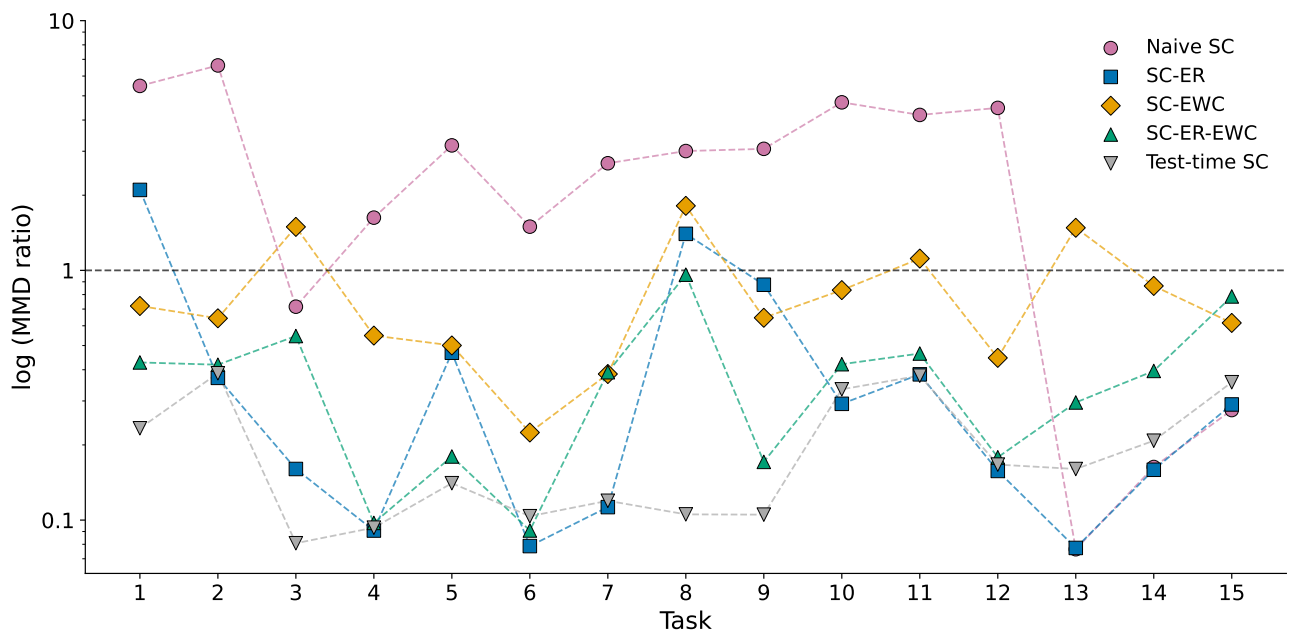


Figure 12: **Experiment 2.** MMD ratio in log scale across CL tasks (1–15) for different methods. Dashed line marks parity with simulation-based (SB) baseline (ratio = 1). Naive SC shows catastrophic forgetting in CL setting whereas our proposed methods mitigate forgetting and provide better posterior estimates compared to SB and Naive SC. Test-time SC also gives accurate posterior estimates.

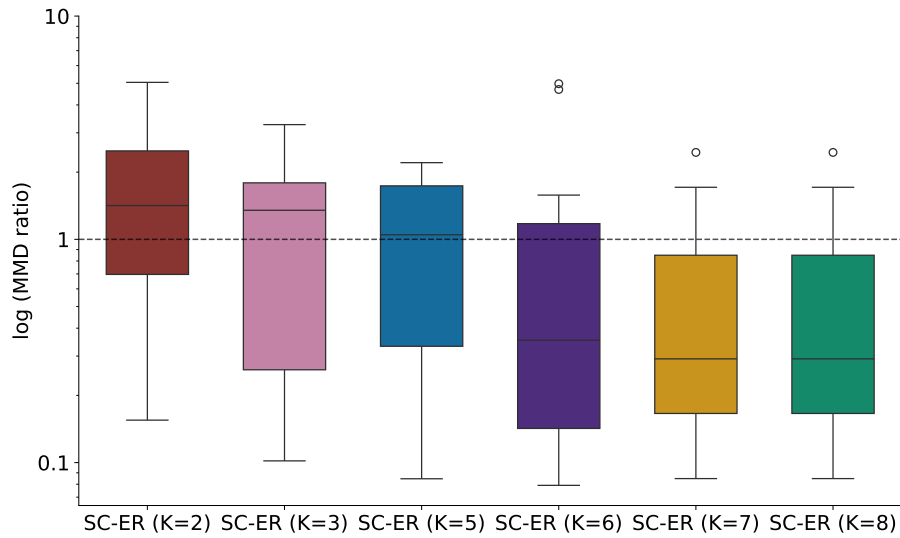


Figure 13: **Experiment 2.** MMD ratio in log scale aggregated over fifteen CL tasks for SC-ER with varying replay memory buffer K . Dashed line marks parity with simulation-based baseline (ratio = 1). For values of $K \leq 6$ the performance of SC-ER starts to decrease whereas for $K \geq 7$, good performance is observed.

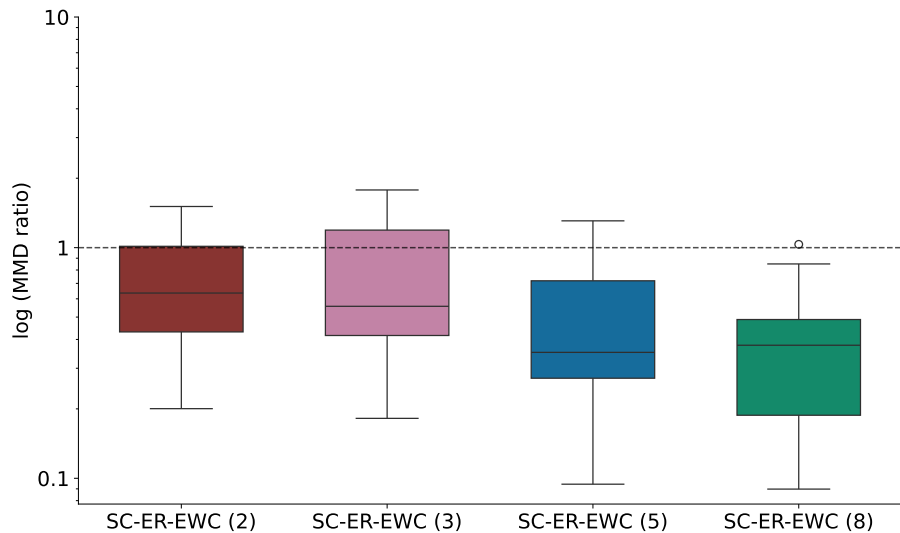


Figure 14: **Experiment 2.** MMD ratio in log scale aggregated over fifteen CL tasks for SC-ER-EWC with varying replay memory buffer K . Dashed line marks parity with simulation-based baseline (ratio = 1). For values of $K = 2, 3$ the performance of SC-ER-EWC decreases but still remain better than SB baseline as well as SC-ER for same K -value. It signifies that addition of EWC leads to enhanced performance when replay memory is limited.

F EXPERIMENT 3: DATASET AND MODEL DESCRIPTION

The eight empirical datasets originally come from studies done by Chetverikov et al. [2017], Hedge et al. [2018], and Pratte et al. [2010] and were extracted from the database provided by Haaf et al. [2025] under the dataset ID numbers: 1, 5, 6, 7, 8, 38, 39, and 40. These datasets contain responses of participants on the Stroop task [Stroop, 1935], Flanker task, [Eriksen and Eriksen, 1974], or Simon task [Simon, 1990]. The number of participants in each data set ranges between 30 and 60. For convenience, we recoded the response time and accuracy data so that incorrect responses are coded as negative response times. Further, we also retained 180 trials per participant (90 congruent and 90 incongruent trials), so that the networks are trained on data with constant sample size.

The racing diffusion model [Tillman et al., 2020] posits that each response alternative (correct vs. incorrect) is represented by its own noisy evidence accumulator. Each accumulator starts at zero and follows a Wiener process with drift (where W_t denotes a standard Wiener process),

$$X_t = \nu dt + \sigma dW_t, \quad X_0 = 0. \quad (17)$$

A response is generated when one of the accumulators first reaches the decision boundary α . The observed response time corresponds to the hitting time of the winning accumulator plus a non-decision time component t_0 . Consequently, the model yields response times (rt , in seconds) together with accuracies (correct/incorrect) on each trial. For training, incorrect responses were encoded as negative values of the associated rt , allowing the networks to condition on a single variable that jointly represents speed and accuracy.

We used the following priors on the parameters,

$$\log \alpha \sim \mathcal{N}(0, 0.5) \quad \log \nu_{\text{correct}} \sim \mathcal{N}(0, 0.5), \quad \log \nu_{\text{incorrect}} \sim \mathcal{N}(0, 0.5), \quad \text{logit } \tau \sim \mathcal{N}(0, 1), \quad (18)$$

with $\sigma = 1$. The parameter τ determines the non-decision time via

$$t_0 = \min(rt) \frac{\tau}{1 - \tau}. \quad (19)$$

This reparameterization allows estimation of $\text{logit } \tau$ on an unconstrained scale while ensuring $t_0 \in (0, \min(rt))$.

Both the neural posterior and neural likelihood estimators are implemented as normalizing flows [Dinh et al., 2016] with six spline coupling layers. Each coupling layer contains two dense layers with 256 hidden units and mish activations [Misra, 2019]. The summary network follows a DeepSet architecture [Zaheer et al., 2017] comprising two equivariant modules (each with two dense layers and 64 hidden units), an invariant module with two dense layers and 32 hidden units in both the inner and outer components, an additional invariant module with two dense layers of 32 hidden units, and an output layer with 30 units. All layers except the output layer use SiLU activations.

SB training followed an online regime (100 epochs, 64 steps per epoch with batch size of 64). SC training consisted of 200 training steps, with each step utilizing the entire data set for computing the SC loss, with the variance target computed over 128 samples from the current posterior approximation [Mishra et al., 2025]. Because the SC loss was unstable, we restored weights of the networks that gave the smallest SC loss during the 200 training steps, to ensure that the results are not affected by a random fluctuation at the final step.

G EXPERIMENT 3: ADDITIONAL RESULTS

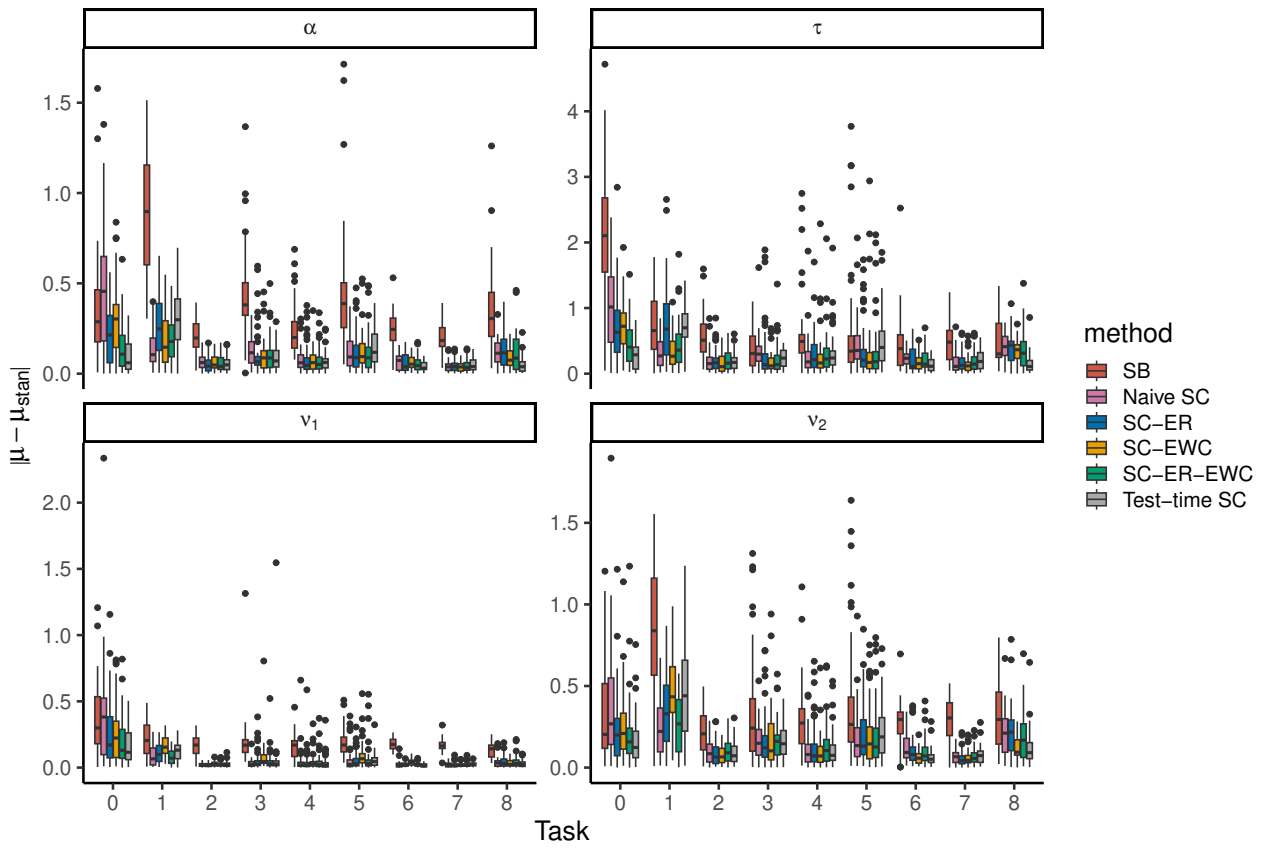


Figure 15: **Experiment 3.** Absolute bias of the posterior mean of the marginal posteriors of the racing diffusion model.

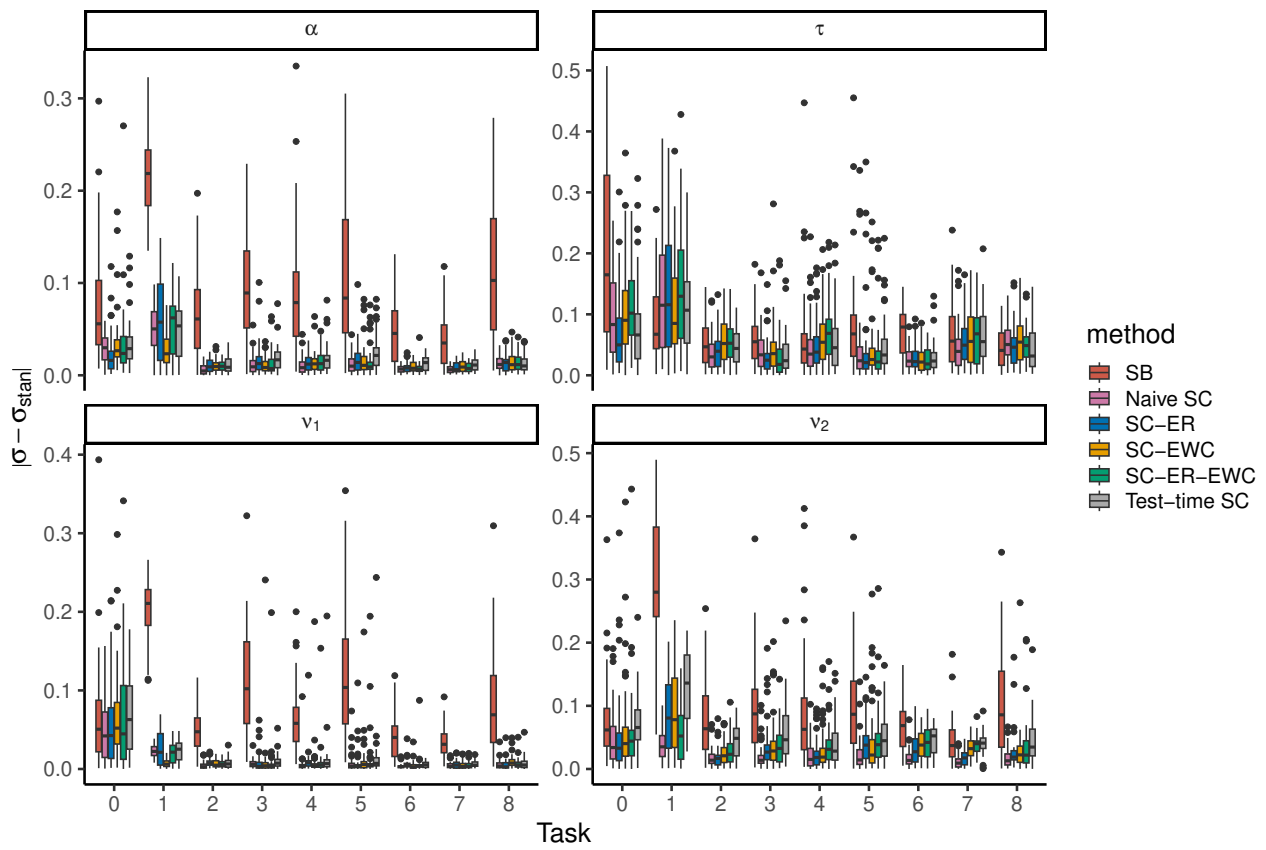


Figure 16: **Experiment 3.** Absolute bias of the posterior standard deviation of the marginal posteriors of the racing diffusion model.